NOTICE

The quality of this microform is heavily dependent upon the quality of the original thesis submitted for microfilming. Every effort has been made to ensure the highest quality of reproduction possible.

If pages are missing, contact the university which granted the degree.

Some pages may have indistinct print especially if the original pages were typed with a poor typewriter ribbon or if the university sent us an inferior photocopy.

Reproduction in full or in part of this microform is governed by the Canadian Copyright Act, R.S.C. 1970, c. C-30, and subsequent amendments.

AVIS

La qualité de cette microforme dépend grandement de la qualité de la thèse soumise au microfilmage. Nous avons tout fait pour assurer une qualité supérieure de reproduction.

S'il manque des pages, veuillez communiquer avec l'université qui a conféré le grade.

La qualité d'impression de certaines pages peut laisser à désirer, surtout si les pages originales ont été dactylographiées à l'aide d'un ruban usé ou si l'université nous a fait parvenir une photocopie de qualité inférieure.

La reproduction, même partielle, de cette microforme est soumise à la Loi canadienne sur le droit d'auteur, SRC 1970, c. C-30, et ses amendements subséquents.

CHARACTERIZATION OF EPITAXIAL CdT AND PbTe LAYERS GROWN BY R.F. MAGNETRON SPUTTERING

By

GOUTAM MUKHERJEE

Thesis submitted to the school
of Graduate Studies of the University of Ottawa
in partial fulfillment of the
requirements for the degree of
Master of Science
in
Physics

DEPARTMENT OF PHYSICS
FACULTY OF SCIENCE
UNIVERSITY OF OTTAWA

ISBN 0-315-60015-2

UNIVERSITÉ D'OTTAWA
UNIVERSITY OF OTTAWA

TO MY PARENTS

ACKNOWLEDGEMENTS

First of all, I would like to express my sincere gratitude to my thesis supervisor Dr. S. R. Das for his guidance, advice, encouragement and help during the course of this work.

The work reported in this thesis was carried out in the Chemical Physics Section of the Microstructural Sciences Laboratory at the Division of Physics, National Research Council (N.R.C.) and thanks are due to the Director of the Division of Physics for permitting me to work at the Laboratory as a guest worker. I especially would like to thank Dr. J. G. Cook, Dr. G.C. Aers and Mr. H. Moeller of the N.R.C. for their cooperation and assistance at all times during this thesis work. Acknowledgement is also extended to all my friends at the Department of Physics, Ottawa University.

Finally, special thanks to my wife Mistu for her encouragement and help during the preparation of the thesis.

ABSTRACT

This thesis reports (i) a study of the temperature dependence of the dark conductivity, the photoconductivity and the photo-Hall effect and the illumination intensity dependence of the photoconductivity in sputter-deposited heteroepitaxial (100) CdTe layers grown at substrate temperatures of 300-325 ^{0}C on freshly cleaved (100) KBr single crystal substrates and (ii) Hall effect measurements on sputter-deposited heteroepitaxial (111) PbTe layers grown under different conditions of substrate temperature and substrate bias on cleaved and chemipolished (111) BaF_2 single crystal substrates.

Sputter-deposited heteroepitaxial layers of (100) CdTe $\parallel$ (100) KBr prepared at growth temperatures of 300-325 ^{0}C are found to be p-type with high dark resistivities on the order of 2×10^5 ohm-cm. The epilayers are highly photoconducting and exhibit photoconductivity to dark conductivity ratios as high as 1.6×10^6 at around 180 K. The photoconductivity σ_{ph}[expressed as $\sigma_{ph} \propto f^{\gamma}$] is observed to exhibit a sublinear ($\gamma \prec 1$) dependence on illumination intensity f. Photo-Hall effect measurements show that the photoconductivity is due to change in carrier concentration and not due to any enhancement in the carrier mobility. Moreover, the photocurrent is carried by holes. From the temperature dependence of the dark conductivity, acceptor levels have been determined at 0.64 eV and 0.08 eV above the valence band. Hole trap levels at $\approx$ 0.4 eV and $\approx$ 0.2 eV above the valence band have been determined from the temperature dependence

of the photoconductivity.

Hall measurements on sputter-deposited epitaxial PbTe films have confirmed that samples prepared at high growth temperatures (330 ^{0}C and 410 ^{0}C) are n-type and those grown at low substrate temperatures (180 ^{0}C and 260 ^{0}C) are p-type, irrespective of the substrate bias applied during growth. However, the carrier concentration values are generally high and do not exhibit a systematic variation with deposition conditions. The Hall mobilities in some of the sputter-deposited films are comparable to values obtained on films with similar carrier concentrations grown by other techniques. The low temperature mobility values in the sputter-deposited samples are found to be limited by a temperature-independent neutral impurity scattering mechanism. The neutral impurities have not been identified but could be structural defects. One of the features of heteroepitaxial growth is the existence of a large density of structural defects at the interface due to lattice mismatch. The density of these defects is observed to decrease with film thickness along the growth direction and thus films with higher thickness exhibit high bulk-like mobilities.

The lack of control on the carrier concentration as well as the mobilities indicate the need to optimize the deposition conditions and grow thicker films. Such an effort is currently underway.

Contents

List of Figures

List of Tables

Chapter 1

Introduction

1.1 Aim Of The Thesis

CdTe[1] and PbTe[2] are important semiconductors with diverse opto-electronic applications and have been extensively investigated in both bulk and thin film form. Epitaxial, monocrystalline layers of CdTe[3–11] and PbTe[12–17,23–27] have been grown by a variety of techniques including molecular beam epitaxy[3–5,23–27], hot-wall epitaxy[6,12–16], laser assisted deposition[7], atomic layer epitaxy[8], ionized cluster beam epitaxy[9], vacuum evaporation[18–21] and photo-assisted deposition[11] However, sputter-deposition has not been

successfully employed to grow single crystal layers of these materials. Recently, workers in the Chemical Physics Section in the Laboratory for Microstructural Sciences of the Division of Physics at the National Research Council of Canada have succeeded in growing epitaxial layers of CdTe[28,34] and PbTe[29] on cleaved single crystal KBr and chemipolished single crystal BaF_2 substrates, respectively, by r.f. magnetron sputtering utilizing low energy ion bombardment during growth to achieve epitaxy. These layers have been structurally characterised by X-ray diffraction, electron diffraction and transmission and scanning electron microscopy and optically by reflectance and transmittance spectroscopy. The results of these structural and optical studies have been reported previously[28,29,30]. This thesis reports the results of a study of the electrical properties of the sputter-deposited epitaxial CdTe and PbTe layers. The CdTe epilayers were observed to be highly photoconducting and the electrical investigations of these layers involved measurement of the temperature and illumination intensity dependence of the dark conductivity and photoconductivity followed by limited Hall effect measurements in dark and under illumination. The PbTe layers were characterised primarily by Hall effect measurements with no illumination.

In the following sections, we give a description of semiconductor statistics, followed by a brief discussion of the transport properties of and the Hall effect in semiconductors and finally a phenomenological description of photoconductivity to provide a conceptual basis for analysing the results of our measurements.

1.2 Semiconductor Statistics

It is necessary, at this point, to consider the band structure of semiconductors, i.e., the energy momentum (E-K) relationship of the electrons in the semiconductor, which is fundamental to the understanding of the electrical and optical properties. The band structure in a solid is determined primarily by the crystal structure. The energy band structure of CdTe and PbTe are depicted in Figure 1.1(a,b).

Semiconductor statistics[31] are derived on the basis of the simple picture of parabolic conduction and valence bands as shown in figure 1.2(a,b). In the intrinsic case, the number of occupied conduction band levels, n, is given by

$$n = \int_{E_c}^{E_{top}} N(E)F(E)dE \tag{1.1}$$

where E_c is the energy at the bottom of the conduction band, E_{top} is the energy at the top, N(E) is the density of states, and F(E) is the Fermi-Dirac distribution function. For low carrier densities and temperatures, N_E can be written as

$$N(E) = M_c[2(E - E_c)]^{1/2}(m_{de})^{3/2}(\frac{1}{\pi^2})(\frac{1}{\hbar^3}) \tag{1.2}$$

where M_c is the number of equivalent minima in the conduction band and m_{de} is the density-of-states effective mass for electrons and can be written as

$$m_{de} = (m_1^* m_2^* m_3^*)^{1/3} \tag{1.3}$$

where m_1^*,m_2^* and m_3^* are the electron effective masses along the principal axes of the ellipsoid energy surface. The electron effective mass is given by

$$m^* = (\hbar^2)/(\delta^2 E/\delta K^2) \tag{1.4}$$

F(E) is given by

$$F(E) = \frac{1}{1 + [\exp(E - E_f)/kT]} \tag{1.5}$$

where k is the Boltzmann constant, T is the absolute temperature and E_f is the Fermi energy. Therefore, n is given by

$$n = N_c(2/\pi^{1/2})F_{1/2}[(E_c - E_f)/kT] \tag{1.6}$$

where N_c is the effective density of states in the conduction band, expressed by the relation

$$N_c = 2(2\pi m_{de} kT/h^2)^{3/2}(M_c) \tag{1.7}$$

The Fermi-Dirac integral is given by $F_{1/2}(n_f)$ with $n_f = (E_c - E_f)/kT$. For nondegenerate semiconductors, E_f is several kT below E_c and $F_{1/2}$ approaches the value $(\pi^{1/2}e^{-n_f})/2$ and so the equation for n becomes

$$n = N_c \exp[-(E_c - E_f)/kT] \tag{1.8}$$

In a similar manner, the hole density, p, near the top of the valence band(E_v) for nondegenerate conditions can be written as

$$p = N_v \exp[-(E_f - E_v)/kT] \tag{1.9}$$

The effective density of states in the valence band is given by

$$N_v = 2(2\pi m_{dh} kT/h^2)^{3/2} \tag{1.10}$$

where m_{dh} is the density-of-state effective mass of the holes in the valence band and is given by

$$m_{dh} = (m_{lh}^{*3/2} + m_{hh}^{*3/2})^{2/3} \tag{1.11}$$

where m_{lh}^* is the light-hole effective mass and m_{hh}^* is the heavy-hole effective mass. At finite temperatures, thermal excitation of electrons from the valence band to the conduction band leads to an equal number of electrons in the conduction band and holes left behind in the valence band. Therefore, we can write $n = p = n_i$. This thermal excitation is balanced by the recombination of electrons in the conduction band with holes in the valence band.

Equating the equations for n and p, the Fermi level for an intrinsic semiconductor can be written as

$$E_f = E_i = [(E_c+E_v)/2]+[(kT)/2]\ln(N_v/N_c) = [(E_c+E_v)/2]+3(kT/4)\ln(m_{dh}/m_{de}) \tag{1.12}$$

Thus, at T=0, the Fermi level lies in the middle of the forbidden gap. With increasing temperature, the Fermi level moves towards the band in which the effective mass for the density of states is less. The intrinsic carrier

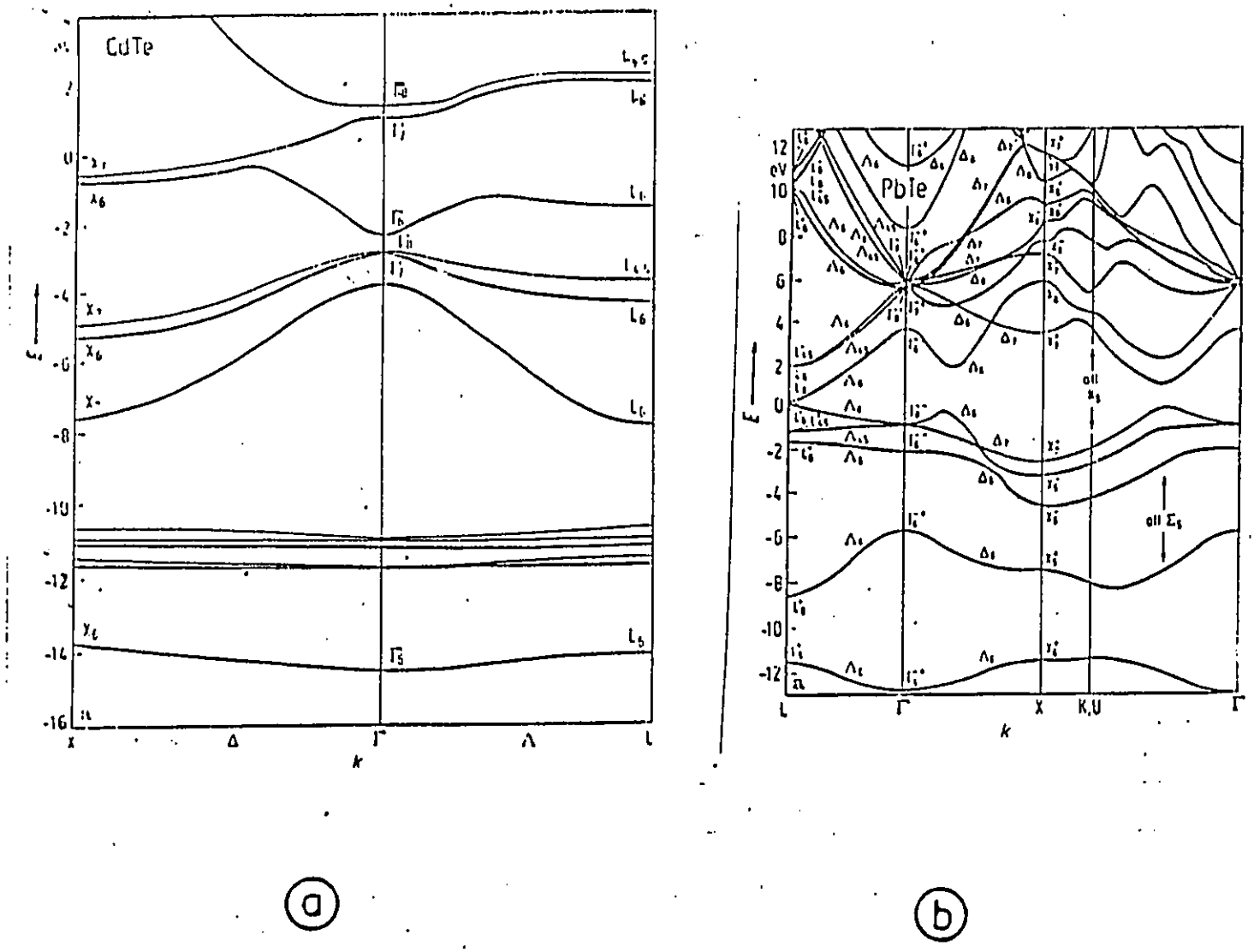

(a) (b)

Figure 1.1: The energy band structure of (a) CdTe and (b) PbTe[37,38]

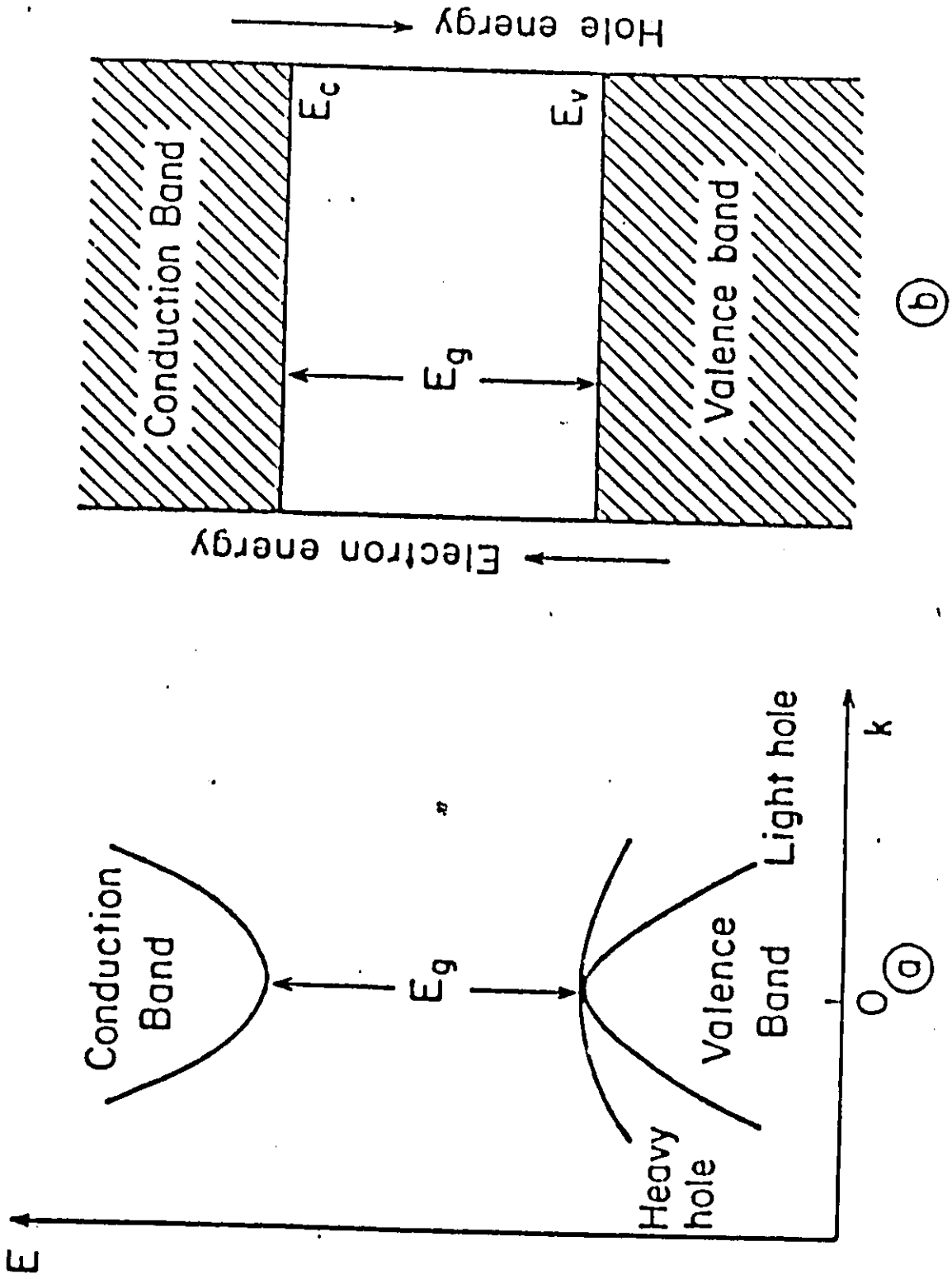

Figure 1.2: Simple picture of parabolic conduction and valence bands

concentration, n_i, can be written as

$$n_i^2 = np = N_c N_v \exp(-E_g/kT) \tag{1.13}$$

where $E_g = E_c - E_v$. Thus, n_i can be written as

$$n_i = (N_c N_v)^{1/2}[\exp(-E_g/2kT)] = 4.9\times10^{15}(m_{de}m_{dh}/m_0^2)^{3/4}T^{3/2}\exp(-E_g/2kT) \tag{1.14}$$

where m_0 is the mass of the free electrons.

Impurity levels can be introduced in a semiconductor by doping the semiconductor with either donors or acceptors. An acceptor level is termed neutral if empty and negative if filled by an electron. A donor level is neutral if it is filled by an electron and positive if it is empty. The impurity levels can be calculated with the help of the hydrogen atom model. The ionization energy of the hydrogen atom, E_H, is given by

$$E_H = m_0 q^4/(32\pi^2\varepsilon_0^2\hbar^2) = 13.6eV \tag{1.15}$$

where q is the electronic charge and ε_0 is the permittivity of free space. The ionization energy of the donors E_d can be calculated by interchanging m_0 by the conductivity effective mass of electrons, m_{ce} and ε_0 by the permittivity of the semiconductor, ε_s, where m_{ce} is given by

$$m_{ce} = 3(\frac{1}{m_1^*} + \frac{1}{m_2^*} + \frac{1}{m_3^*})^{-1} \tag{1.16}$$

Thus, using the equation for E_H, E_d can be written as

$$E_d = (\varepsilon_0/\varepsilon_s)^2(m_{ce}/m_0)E_H \tag{1.17}$$

In a similar way, the ionization energy E_a for acceptors can be calculated. With introduction of impurity atoms, the Fermi level adjusts itself to preserve charge neutrality. If $N_d(cm^{-3})$ donors are introduced into the semiconductor, then charge neutrality requires

$$n = N_d^+ + p \tag{1.18}$$

where n is the electron density in the conduction band, p is the hole density in the valence band and N_d^+ is the number of ionized donors given by

$$N_d^+ = N_d[1 - \frac{1}{1 + (1/g)\exp[(E_d - E_f)/kT]}] \tag{1.19}$$

Similarly, for acceptors we can write

$$N_a^- = N_a[\frac{1}{1 + (1/g)\exp[(E_a - E_f)/kT]}] \tag{1.20}$$

where g is the ground state degeneracy factor. The values of g for donors and acceptors are 2 and 4, respectively. The Fermi level can be determined by using the above charge neutrality equation :

$$N_c \exp[-(E_c - E_f)/kT] = N_d[\frac{1}{1 + 2\exp[(E_f - E_d)/kT]}] + N_v \exp[(E_v - E_f)/kT] \tag{1.21}$$

Thus for a given set of N_c, N_d, N_v, E_c, E_d, E_v and T, the Fermi level can be uniquely determined. For n type semiconductors, at low temperatures,

the Fermi level rises towards the donor level and the donor level is partially filled with electrons. The electron density can be written as

$$n \simeq [(N_d - N_a)/2N_a]N_c \exp(-E_d'/kT) \tag{1.22}$$

for $N_a \gg (1/2)N_c \exp(-E_d'/kT)$, where $E_d' \equiv (E_c - E_d)$, or

$$n \simeq (1/2^{3/2})(N_d N_c)^{1/2} \exp(-E_d'/2kT) \tag{1.23}$$

for $N_d \gg (1/2)N_c \exp(-E_d'/kT) \gg N_a$. At high temperatures, $n \approx p \gg N_d$ and the intrinsic region is observed. At very low temperatures, most impurities are frozen out and the carrier concentration is given by equation 1.22 or equation 1.23 In the intermediate temperature range, the electron density remains essentially constant.

It should be noted that even when impurity atoms are added, the np product is still given by n_i^2 and is independent of the added impurities. At elevated temperatures, when most of the donors and acceptors are ionized, the neutrality condition can be approximated by

$$n + N_a = p + N_d \tag{1.24}$$

From equation(1.13) and (1.24), the concentrations of electrons n_{n_0} and holes p_{n_0} in an n-type semiconductor can be written as

$$n_{n_0} = (1/2)[(N_d - N_a) + [(N_d - N_a)^2 + 4n_i^2]^{1/2}] \tag{1.25}$$

If $|N_d - Na| \gg n_i$ and $N_d \gg N_a$

$$n_{n_0} \approx N_d \tag{1.26}$$

And for holes

$$p_{n_0} = n_i^2/n_{n_0} \approx n_i^2/N_d \tag{1.27}$$

The subscripts n and p refer to the type of semiconductors and 0 refers tc the thermal equilibrium condition.

Therefore, we can write

$$E_c - E_f = kTln(N_c/N_d) \tag{1.28}$$

From equation(1.12),

$$E_f - E_i = kTln(n_{n_0}/n_i) \tag{1.29}$$

Similarly, for a p-type semiconductor, the hole p_{p_0} and electron n_{p_0} concentrations are given by:

$$p_{p_0} = (1/2)[(N_a - N_d) + [(N_a - N_d)^2 + 4n_i^2]^{1/2}] \tag{1.30}$$

If $|(N_a - N_d)| \gg n_i$ and $N_a \gg N_d$

$$p_{p_0} \approx N_a \tag{1.31}$$

$$n_{p_0} = n_i^2/p_{p_0} \approx n_i^2/N_a \tag{1.32}$$

and

$$E_f - E_v = kTln(N_v/N_a) \tag{1.33}$$

or

$$E_i - E_f = kTln(p_{p_0}/n_i) \tag{1.34}$$

For degenerate semiconductors, i.e., E_f lying inside an energy band close to or higher than 5kT away from the energy extremum, the electron concentration is independent of temperature and is given by the equation

$$n = [8\pi/3](2m_{de}/h^2)^{3/2}(E_f - E_c)^{3/2} \tag{1.35}$$

The hole concentration when the Fermi level lies more than 5kT below E_v is given by the temperature-independent expression

$$p = [8\pi/3](2m_{dh}/h^2)^{3/2}(E_v - E_f)^{3/2} \tag{1.36}$$

In an n-type material where $n_{n_0} \succ p_{p_0}$, electrons are called majority carriers and holes are called minority carriers. The reverse is true for p-type semiconductors.

1.3 Transport Properties Of Semiconductors

In this section we are going to discuss the transport properties of semiconductors. At low electric fields, the drift velocity v_d is proportional to the electric field strength E. Therefore, we can write $v_d = \mu E$, where the proportionality constant μ is defined as the mobility of the carrier. The mobility is dependent on various scattering mechanisms[31,32], each of which is dominant in a particular temperature range. The scattering can be due to (i)thermal lattice vibration or phonons, (ii)impurity ions, (iii)impurity atoms, (iv)vacancies and point defects, (v)dislocations, (vi)grain boundaries, cleavage planes and crystal surfaces, and (vii)charge carriers.

For the case of thermal lattice vibration scattering (acoustic phonons) the mobility,μ_L, can be written as

$$\mu_L(T) = [2(2\pi)^{1/2}\rho\hbar^4 s^2|e|]/[2E_1^2 m^{*5/2}(kT)^{3/2}] \tag{1.37}$$

where e, $\hbar$, and k are universal constants; ρ is the mass density, s is sound velocity, E_1 is the acoustic phonon deformation potential in eV, m^* is the effective mass and T is the temperature. In a given solid, mobility depends only on temperature as

$$\mu_L \simeq \mu_0 T^{-3/2} \tag{1.38}$$

In the case of optical lattice vibration scattering(optical phonons),

$$\mu_L \propto m^{*-3/2}[\exp(\hbar w_0/kT) - 1] \tag{1.39}$$

where w_0 is the optical frequency.

Ionized impurity scattering mobility,μ_I, is given by

$$\mu_I = 8(2^{1/2}k^{3/2}\varepsilon^2 T^{3/2})/\pi^{3/2}e^3 Z^2 N_I m^{*1/2}[\ln(1 + 3\varepsilon kT/N_I^{1/3}Ze^2)^2] \tag{1.40}$$

where N_I is the number of impurity ions, Z is the atomic number and ε is the permittivity. At high temperatures, neglecting the logarithmic dependence on temperature,

$$\mu_I \approx \mu_{0I} T^{3/2} \tag{1.41}$$

As the temperature decreases, the mobility due to impurity ion scattering also decreases as

$$\mu_I \simeq 1/(T^{1/2}) \tag{1.42}$$

For scattering by N_n neutral centers the mobility has the form

$$\mu_n = e^3 m^*/(20\varepsilon\hbar^3 N_n) \tag{1.43}$$

For dislocation scattering

$$\mu \approx (\frac{1}{T})^{1/2} \tag{1.44}$$

The electron transport properties of thick epitaxial semiconducting films with bulk or nearly bulk-like properties may be characterized by the resistivity, Hall coefficient, and Hall mobility. Electrical conduction, in general, is determined by various overlapping scattering mechanisms. By analogy with Mathiessen's rule, the total mobility, μ_F, is given by

$$1/\mu_F = 1/\mu_L + 1/\mu_I + 1/\mu_s + 1/\mu_n \tag{1.45}$$

where μ_L, μ_I, μ_s and μ_n are contributions due to lattice, impurity, surface(including grain boundary) and neutral centers scattering, respectively. In general, the additive effect of various overlapping scattering mechanisms gives rise to a complicated temperature dependence.

1.4 The Hall Effect

Conductivity measurements alone are not sufficient for the determination of the number of conducting charges (n,p) and their mobility μ. Moreover,

these measurements do not give any information about the type of the charge carriers. Hall effect measurements supply the information on the sign of the charge carriers.

If an external electric field is applied along the axis of a specimen, then the electrons will drift in the opposite direction. In addition to that, if a magnetic field is applied perpendicular to the axis of the specimen, the electrons will tend to be deflected to one side. As a result of this, a surface charge will develop. The surface charge then gives rise to a transverse electric field which causes a compensating drift such that the carriers remains in the specimen. This effect is known as the Hall effect.

Consider a slab of material subjected to an external electric field E_x along the x-direction and a magnetic field H_z along the z-direction. Due to the electric field a current density I_x will flow in the direction of E_x. For an n type material, under the influence of the magnetic field, the electron will be subjected to a Lorentz force such that the upper surface collects a positive charge while the lower surface a negative charge. Ultimately, a stationary state is reached when the current along y-axis vanishes and a field E_y is set up. If the charge carriers are holes, these will be reversed. This voltage in the y-direction is called the Hall voltage.

The electric force on the electron having a charge -e is -eE and the force due to the magnetic field $H = -(e/c)(v \times H)$. Due to the combined effect of electric and magnetic fields, the total force is given by

$$F = -eE - [e/c](v \times H) \tag{1.46}$$

In our case

$$F_y = -eE_y + [e/c](v_x \times H_z) \tag{1.47}$$

In the steady state $F_y = 0$, hence

$$E_y = (1/c)v_x H_z \tag{1.48}$$

This E_y is called the Hall voltage.

Now the current density is given by

$$I_x = N(-e)v_x \tag{1.49}$$

where N is the number of charge carriers. Therefore,

$$v_x = -I_x/Ne \tag{1.50}$$

Thus substituting the value of v_x we get

$$E_y/(I_x H_z) = -1/(cNe) = R_{Hall} \tag{1.51}$$

R_{Hall} is known as the Hall coefficient. The above equation shows that the sign of the Hall constant is the same as the sign of the carrier.

Tables 1.1, 1.2 and 1.3 give some of the bulk properties of CdTe and PbTe. The electron density-of-state effective mass m_e^* for CdTe was calculated from the equation

$$m_e = (m_1^* m_2^* m_3^*)^{1/3} \tag{1.52}$$

Structure	Lattice constant $\AA$	Band gap E_g(eV)	dE_g/dT $(10^{-4}eVK^{-1})$	Electron Effective mass in units of m_0	Hole Effective mass in units of m_0
F.C.C. Zinc blende	6.482	1.475	-3.58	0.0949	0.8207

Table 1.1: Energy band parameters of CdTe

where m_1^* corresponds to the effective mass in the $\prec 110 \succ$ direction, m_2^* corresponds to the effective mass in the $\prec 111 \succ$ direction and m_3^* corresponds to the effective mass in the $\prec 100 \succ$ direction. For holes, the density-of-state effective mass was calculated from

$$m_h = (m_1^* m_2^* m_3^*)^{1/3} \tag{1.53}$$

where

$$m_{1,2,3}^* = [(m_{lh}^*)^{3/2} + m_{hh}^*)^{3/2}]^{2/3} \tag{1.54}$$

for $\prec 110 \succ, \prec 111 \succ$ *and* $\prec 100 \succ$ direction, respectively. The electron and hole effective masses for PbTe were calculated from the following equations

$$m_{||}, n(T) = [30.58E_g(0)/(10.25E_g(T) + 2.42)]^{-1} m_0 \tag{1.55}$$

$$m_{\perp}, n(T) = [30.58E_g(0)/(E_g(T) + 14.29)]^{-1} m_0 \tag{1.56}$$

$$m_{\perp}, p(T) = [30.58E_g(0)/(E_g(T) + 10)]^{-1} m_0 \tag{1.57}$$

$$m_{||}, p(T) = [30.58E_g(0)/(10.25E_g(T) + 1.25)]^{-1} m_0 \tag{1.58}$$

$$E_g(T) = [171.5 + (12.8)^2 + 0.19(T + 20)^2]^{1/2} \tag{1.59}$$

Structure	Lattice	Band gap	dE_g/dT	Electron effective mass		Hole effective mass	
	constant $\AA$	$E_g(ev)$	$10^{-4}eVK^{-1}$	$m_{\|\|}$,n	$m_{\perp}$,n	$m_{\|\|}$,p	$m_{\perp}$,p
F.C.C. Nacl Structure	6.462	0.3961	4.5	0.2010	0.0247	0.2628	0.0276

Table 1.2: Energy band parameters of PbTe

The quoted values of tables 1.1, 1.2 and 1.3 are collected from references 37,38 and 50.

Material	Dielectric constant $\varepsilon(0)$ $(10^{10}Nm^{-2})$	Dielectric constant $\varepsilon(\alpha)$ $(10^{10}Nm^{-2})$	Density gm/cm^3	Co-efficient of linear thermal expansion K^{-1}	Ionic Charge in units of e
CdTe	10.2	7.1	5.87	$4.7 - 4.9 \times 10^{-6}$	0.32
PbTe	414	33	8.242	1.98×10^{-5}	0.18

Table 1.3: Some physical constants of CdTe and PbTe.

1.5 Photoconductivity

Photoconductivity results when absorption of light increases the values of dark free-carrier densities n and p and/or the dark mobilities μ_n and μ_p. Thus

$$\Delta\sigma = e(\Delta n\mu_n + \Delta p\mu_p) \tag{1.60}$$

$$\Delta\sigma = e(n\Delta\mu^*_{bn} + p\Delta\mu^*_{bp}) \tag{1.61}$$

The change in mobility on illumination can occur if the material is inhomogeneous in which case n and p are not uniform throughout.

The following discussion of photoconductivity is taken from ref.(33). Consider an insulator of unit cross-sectional area exposed to a uniform volume excitation which generates free electrons at the total rate of F per second. The total number of photogenerated free electrons in the steady state will be given by

$$\Delta n = F\tau \tag{1.62}$$

where τ is the life time of the free electron. If the electron is trapped and thermally re-emitted to the conduction band, the time spent in traps is not included in τ. The photocurrent will be

$$I = (\Delta ne)/T_r \tag{1.63}$$

where T_r is the transit time of the free electron from cathode to anode. Putting the value of Δn from equation 1.62 in equation 1.63 we get

$$I = eF\tau/T_r \tag{1.64}$$

or

$$I = eFG \tag{1.65}$$

where $G = \tau/T_r$ is the photoconductive gain. It is equal to the number of electrons passing through the photoconductor per excitation or absorbed photon. The transit time is given by

$$T_r = L/v_d = L/E\mu = L^2/V\mu \tag{1.66}$$

where v_d is the drift velocity, E is the electrical field, μ is the mobility of free electrons, L is the spacing of the electrodes and V is the applied voltage. Using equation 1.66, equation 1.65 can be written as

$$I = e(F\mu\tau/L^2)V \tag{1.67}$$

From equation 1.67, we conclude that the photocurrent should increase linearly with applied voltage, assuming that neither the lifetime nor the mobility are voltage dependent. The photoconductivity gain can be made indefinitely large either by increasing the voltage or by decreasing the electrode spacing. However, when the voltage reaches a value given by

$$VC = \Delta ne \tag{1.68}$$

where C is the parallel plate capacitance of the electrodes per unit cross-sectional area of sample, a new physical phenomenon intervenes. A space charge of electrons equal in number to the photoexcited electrons is forced into the photoconductor by the applied field. Higher voltages increase this space charge proportionately. At and above this voltage, the transit time of the electrons become equal to the dielectric relaxation time of the photoconductor and both decrease with increasing voltage.

We know that when photons of energy greater than the energy gap are absorbed in the crystal, free electron-hole pairs are produced. Once the electrons and holes have been produced by the absorption of photon of sufficient energy, they will remain free until they are captured at an imperfection. These capturing centers are of two types: (i) if the captured carrier has a greater probability of being thermally re-excited to a free state than that of combining with a carrier of opposite sign at the imperfection then such capturing centers are called trapping centers (ii) on the other hand, if the captured carrier has a greater probability of combining with a carrier of opposite sign at the imperfection than that of being re-excited to the free state, then these capturing centers are called recombination centers.

Four cases of recombination and trapping processes in semiconductors[32,33] may be considered:

(i) single set of recombination centers(N_r) at low light ($n_r, p_r \succ n, p$)

$$n = f\tau_n = f/(p_r v s_n) \tag{1.69}$$

and

$$p = f\tau_p = f/(n_r v s_p) \tag{1.70}$$

where n is the free electron volume density (optically excited), p is the free hole volume density (optically excited), n_r and p_r are the electron occupied and hole

occupied recombination centers volume density, respectively, τ_n and τ_p are the free electron and free hole life times, respectively, f is the number of excitation per cm^3 per second, v is the thermal velocity, and s_n, s_p are the capture cross-section of recombination centers for free electron and free hole, respectively. From equation 1.69 and 1.70, we can see that the life time of a free electron is independent of and, consequently, in general not equal to the life time of a free hole.

(ii) single set of recombination centers(N_r) at high light ($n, p \succ n_r, p_r$) Under this condition, the free electron and free hole densities must be closely equal, since any difference in n, p must be taken up by the change in occupancy of the recombination centers and the latter density is, by assumption, small compared with n and p. Hence $\tau_n = \tau_p$. It is clear that the occupancy of the recombination centers is modified from n_r, p_r to $n_r^{'}, p_r^{'}$ to fit the condition n=p.

(iii) single set of recombination centers(N_r) and of traps(N_t, P_t) at low light ($n_r, p_r \succ n + n_t, p + p_t$)

This model is the same as the previous one except that a level of electron-trapping states(Etn) and a level of hole-trapping states(E_{tp}) have been added. Electron-trapping states are in thermal contact with the conduction band. This means their occupancy is related to the conduction band by the Boltzmann factor and is given by

$$n_t = n(N_t/N_c)exp(|E_{t:}, E_c|/kT) \tag{1.71}$$

Similarly,

$$p_t = p(P_t/N_v)exp(|E_{tp}, E_v|/kT) \tag{1.72}$$

The life time τ_n and τ_p are invariant with light intensity and insensitive to temperature. The new element added is due to the fact that the response time is now no longer equal to life time, but is greater than the life time by a factor $(1 + n_t/n)$ for electrons and $(1 + p_t/p)$ for holes.

(iv) single set of recombination centers(N_r) and of traps(N_t, P_t) at low light $(n + n_t, p + p_t \succ n_r, p_r)$

The arguments in case (ii) hold for this model as well and lead to the conclusion

$$\tau_n = \tau_p = 1/[N_r v s_p s_n/(s_n + s_p)] \tag{1.73}$$

Also, by the argument of case (iii), the response times are

$$\tau_{on} = \tau_n(1 + n_t/n) \tag{1.74}$$

$$\tau_{op} = \tau_p(1 + p_t/p) \tag{1.75}$$

The response times are invariant with light intensity and approach the common lifetime at increasing temperature at the respective rates $exp(|E_{tn}, E_c|/kT)$ for electrons and $exp(|E_{tp}, E_v|/kT)$ for holes.

The variety of dependencies of photocurrent on light intensity and temperature is substantially unlimited. Photocurrents have been observed to increase linearly, supralinearly and sublinearly with increasing light intensity. Similarly, photocurrents have been observed to be insensitive to temperature as well as to increase or decrease with increasing temperature. The dependence of n and τ_0 on f and T has been calculated by Rose[33] for a variety of possible trap distributions in energy. The results of the calculations are summarized in Table 1.4 taken from ref(32). The following facts need mention:

n vs f. The variation of n vs $f^{1/2}$ expected for a trap-free material becomes a linear variation of n with f for a material with a uniform distribution of traps. A variation of n vs $f^{1/2}$ can be found even with trapping, if the density of photoexcited electrons trapped above the electron Fermi level is greater than the density of photoexcited electrons trapped below the Fermi level. A variation of n with a power of f between 1/2 and 1 can be explained by assuming an exponential

distribution of traps, the density of traps of energy E decreasing exponentially with the distance E from the bottom of the conduction band. Thus, in the range of light intensities for which the density of free carriers is less than the density of trapped carriers, this simple model provides an explanation for n varying with power of f between 0.5 and 1.0. For high light intensities, when the density of free carriers is greater than the density of the density of trapped carriers, bimolecular recombination predominates and n varies as $f^{1/2}$.

n vs T. For many photoconductors, the photocurrent is essentially independent of temperature, at least over large variation of temperature. Such behaviour is to be expected from the model involving a uniform trap distribution. For an exponential trap distribution of the form, $n_E dE = Aexp(-E/kT_1)dE$, the variation of photocurrent with temperature is more rapid, the photocurrent increasing by an order of magnitude for each increase of 100^0, if T_1 is set equal to 1000 K, or by a factor of three for each increase of $100\ ^0$, if T_1 is set equal to 2000 K. For the special case of a greater density of carriers trapped above the Fermi level than below, a rapid exponential variation of photocurrent is predicted, the photocurrent increasing with increasing temperature.

The organisation of the subsequent chapters of this thesis is as follows: Chapter 2 contains a brief description of the film deposition apparatus and details of the experimental techniques employed to measure the temperature dependence of dark conductivity and photoconductivity, the intensity dependence of photoconductivity and the photo-Hall effect in CdTe and the Hall effect in PbTe; in Chapter 3, we discuss the electrical properties of CdTe thin films grown by other techniques and then compare these with our results. The photo-Hall measurements and photoconductivity results for CdTe samples are discussed in detail. The temperature dependence of carrier concentration, Hall mobility, Hall constant

and photoconductivity from temperatures ranging from 77 K to 400 K are discussed and analysed. in Chapter 4, the electrical properties of the PbTe samples, measured in the temperature range 77 K to 300 K are discussed in relation to the growth conditions.

Case	n vs. f	n vs. T
Fermi level in midst of uniform trap distribution. Density of traps in dE, $n_E\,dE$	$n = \dfrac{f}{vS_nN_r}$ $N_r \approx$ constant	Insensitive
Fermi level above uniform trap distribution	$n = \dfrac{f}{vS_nN_r}$ $N_r \approx$ constant	Insensitive
Fermi level below uniform trap distribution, extending from bottom of conduction band to E_0 below bottom of conduction band	$n = \left[\dfrac{f}{vS_n\alpha(T)}\right]^{1/2}$ $\alpha(T) = \dfrac{n_E kT}{N_c}\exp\left(\dfrac{E_0}{kT}\right)$	$n \propto T^{-1/2}\exp\left(-\dfrac{E_0}{2kT}\right)$
Fermi level in midst of an exponential trap distribution. $n_E\,dE = A\exp\left(-\dfrac{E}{kT_1}\right)dE$	$n = \left[\dfrac{f}{vS_nAT_1N_c^{-T/T_1}}\right]^{T_1/(T+T_1)}$ $T < T_1$	$n \propto N_c^{T/(T+T_1)}$

Table 1.4: Temperature and illumination dependencies of photoexcited carriers for one-carrier model with trapping.

Chapter 2

Experimental Techniques

2.1 R.F. Magnetron Sputter Deposition System

A schematic diagram of the sputtering apparatus is shown in fig.2.1 and an expanded view of the cathode and substrate holder assembly is shown in fig.2.2. The non-magnetic, 66 cm diameter, 25.4 cm high stainless steel sputtering chamber (Materials Research Corporation Model 8667) provides three magnetron cathodes (labelled cathode 1, cathode 2, cathode 3) mounted 90 degrees apart on a 71 cm diameter stainless steel top plate. The targets, bonded to the cathodes, consist of hot-pressed 99.999 % pure CdTe and PbTe discs, 0.6 cm thick and of 16.5 cm diameter. Substrates are placed on a heater block supported on a large annular table which can be either rotated continuously or stepped down to discrete posi-

tions below the targets. Also, the substrates can be heated or sputter-etched prior to deposition. Up to four individual stainless steel shutters are provided. Position indicators and position locks assure correct location of the shutters. The function of these shutters is to prevent the sputtered species from depositing on the substrate during pre-sputtering. The RF generator is an MRC model S3013 and its frequency is 13.56 MHz. The magnetron cathodes are constructed of stainless steel and copper with waterflow concentrated over areas of high power density.

The sputtering chamber is pumped down by using a rotary pump, a varian V80 turbo molecular pump, an NRC made liquid nitrogen trap and a CTI CRYOTORR 8 cryo-pump. The latter provides fast, clean pumping of all gases in the 10^{-3} to 10^{-10} Torr range. A varian 843 vacuum ionization gauge reads the pressures in the above range while a THERMOVAC TM 2105 reads the higher pressures. The flow of the sputtered gas(UHP Ar) is controlled by an MKS mass flow controller.

For CdTe, the substrates used were (100) freshly cleaved single crystal KBr. For PbTe, (111) oriented, freshly cleaved and chemipolished single crystal BaF_2 substrate were used. The substrates were attached to the heater block using a dag solution for KBr or InGa alloy for BaF_2.

Typical depositions conditions for growing CdTe epilayers on KBr were: substrate temperature of 300-325 ^{0}C, r.f. power $\approx$ 50-100 W, Ar flow rate of 80-100 sccm(standard cubic cm per minute) and sputter pressure of 3.5 mTorr. With these deposition conditions the rate of deposition was 3-5 $\mathring{A}/s$[28]. PbTe epilayers on BaF_2 were grown at substrate temperatures between 180-400^{0}C. The r.f. power used was approximately 40-50 W. The Ar flow rate was 80-100 sccm giving a sputter pressure of 4.0 mTorr. A substrate bias of -10 V was employed during deposition. Under the above conditions, growth rates up to 2.5 μ/h were

obtained[29].

2.2 Ohmic Contacts

Ohmic contacts are essential to perform electrical measurements. On all our samples of CdTe, ohmic contacts were made by evaporating gold on the samples in a vacuum system at a pressure of 10^{-6} torr. Then these samples were annealed at a temperature of 150 ^{0}C for 1 hour. Ohmic contacts to PbTe were made by evaporating In or Au on the samples and then annealing at 100 ^{0}C for 1 hour. The ohmic nature was checked by taking current-voltage (I-V) measurements, with different voltages from -15 V to 15 V. For the I-V measurements, a Keithley 617 programmable electrometer was used as shown in figure 2.3(b). The voltage supplied from the voltage source of the electrometer, was varied in small intervals of 0.05 V in the low voltage region(0.1 V to 1.0 V or -0.1 V to -1.0 V). For each voltage, the resistance of the samples was measured in the V/I mode of the electrometer. Then, from the plot of V versus I, the ohmic nature of the samples was verified.

2.3 Sample Mounting

Electrical measurements were done over the temperature range 77-400 K in vacuum using a Janis cryostat. The samples were mounted inside the cryostat on a cold finger exactly in the middle of the two magnetic pole pieces N and S, as shown in figure 2.4. The electrical connections were taken through the electrical feedthrough of the cryostat. High resistance cables were used for all the connections. The cryostat could be pumped down to 10^{-5} Torr by a diffusion pump system. A magnetic field of 2.5 KG was applied to the samples for Hall effect measurements. The magnetic field was measured by placing a gaussmeter exactly at the center of the pole pieces when a fixed voltage and current was applied through the magnet power supply. The samples were cooled down to 77 K by passing liquid N_2 through the cold finger. By passing current through a resistance heater (embedded in the cold finger) while maintaining the cryogen flow, the desired temperature could be achieved. Also, the cryostat had an illumination facility to perform photoconductivity and photo-Hall effect measurements for CdTe samples. A tungsten halogen lamp was used to illuminate the samples through the optical window. A mirror was placed at an angle of 45^0 to reflect the light rays from the tungsten lamp to illuminate the entire sample. Several neutral density filters were used to perform the photoconductivity and photo Hall effect measurements at different light intensities. The illumination intensities were calculated by measuring the transmission of the neutral density filters in a spectrometer.

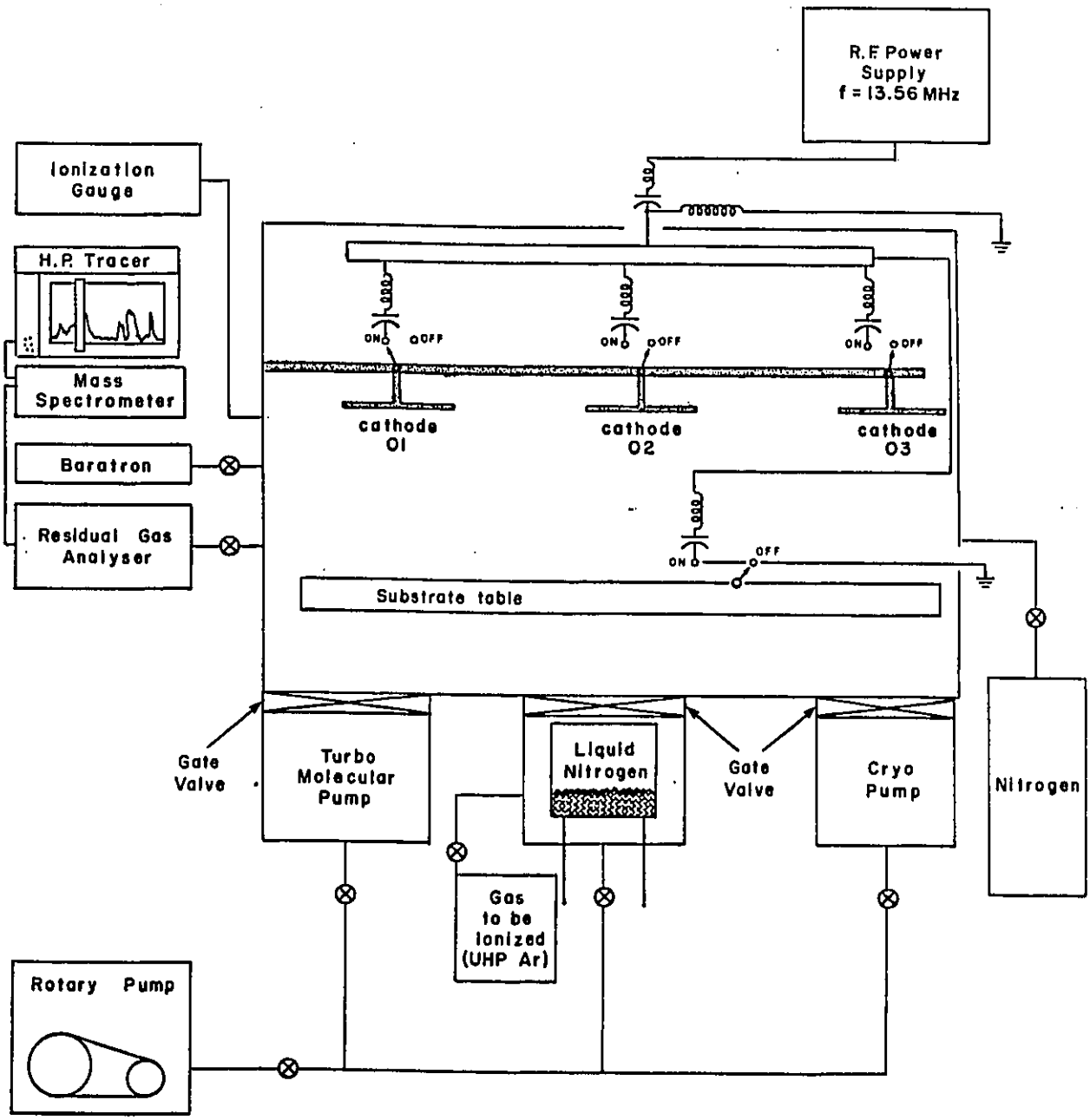

Figure 2.1: Schematic of the sputtering apparatus

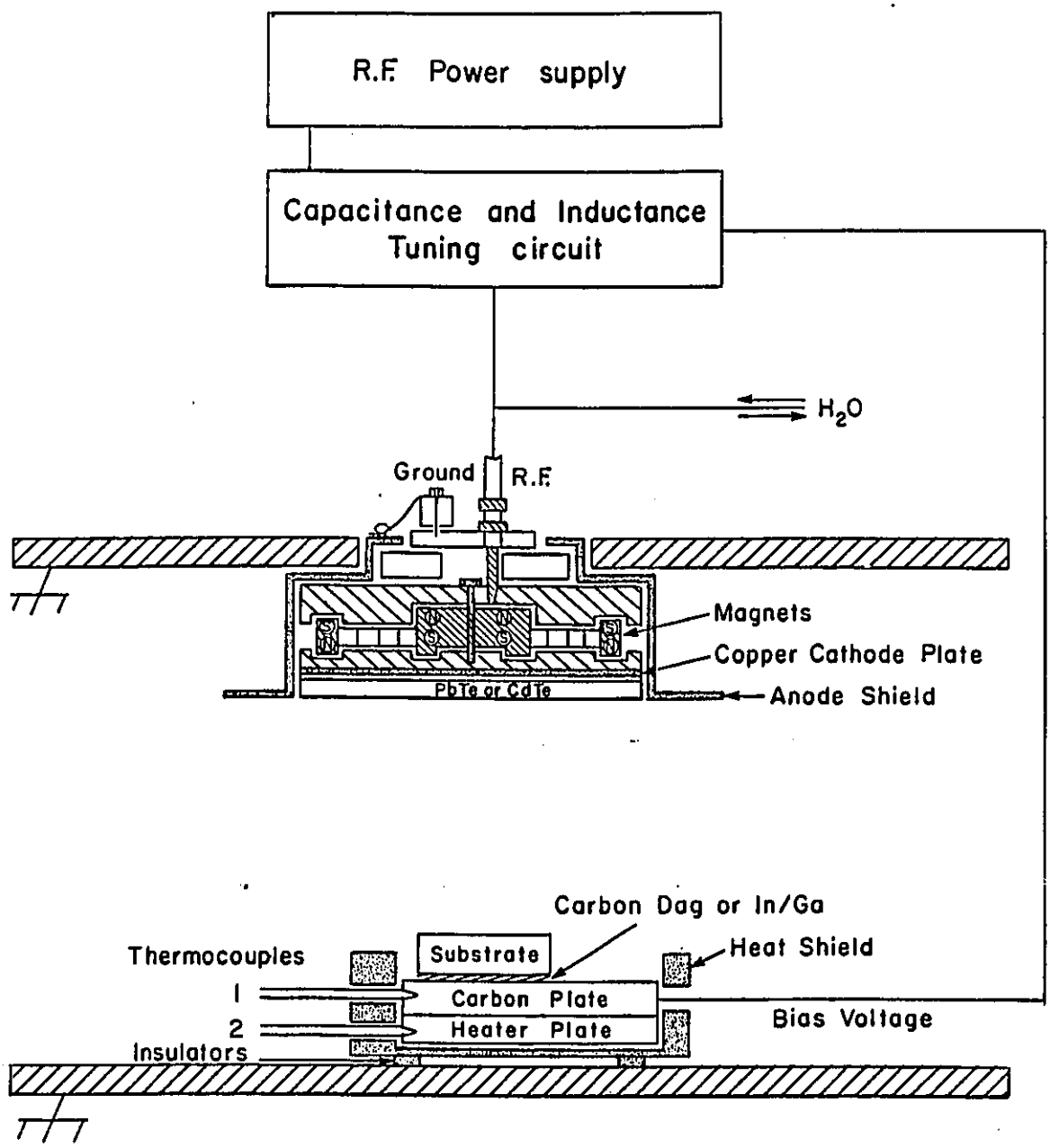

Figure 2.2: Schematic of a magnetron cathode

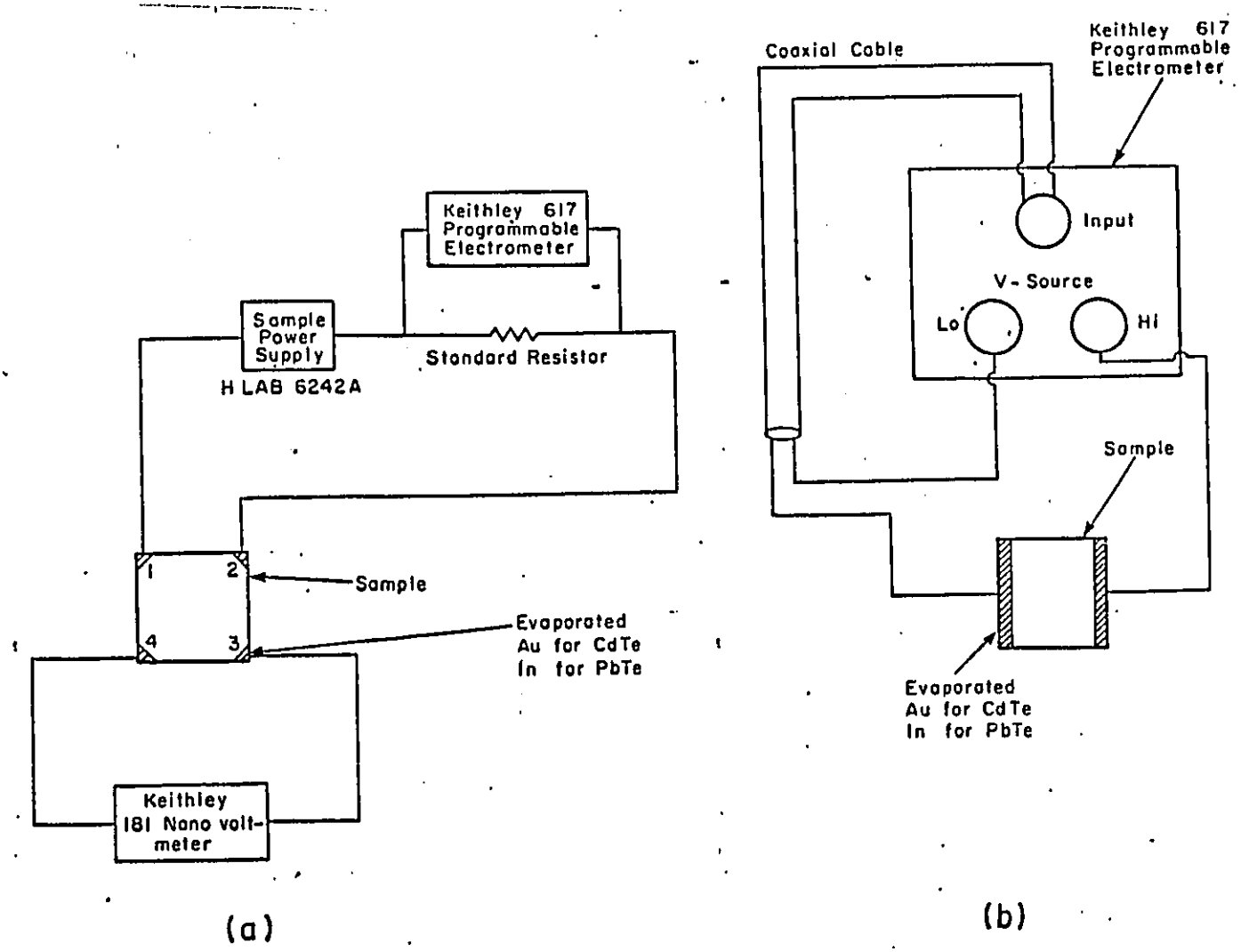

Figure 2.3: Circuit diagram of (a) the Hall effect measurements and (b) photoconductivity measurements

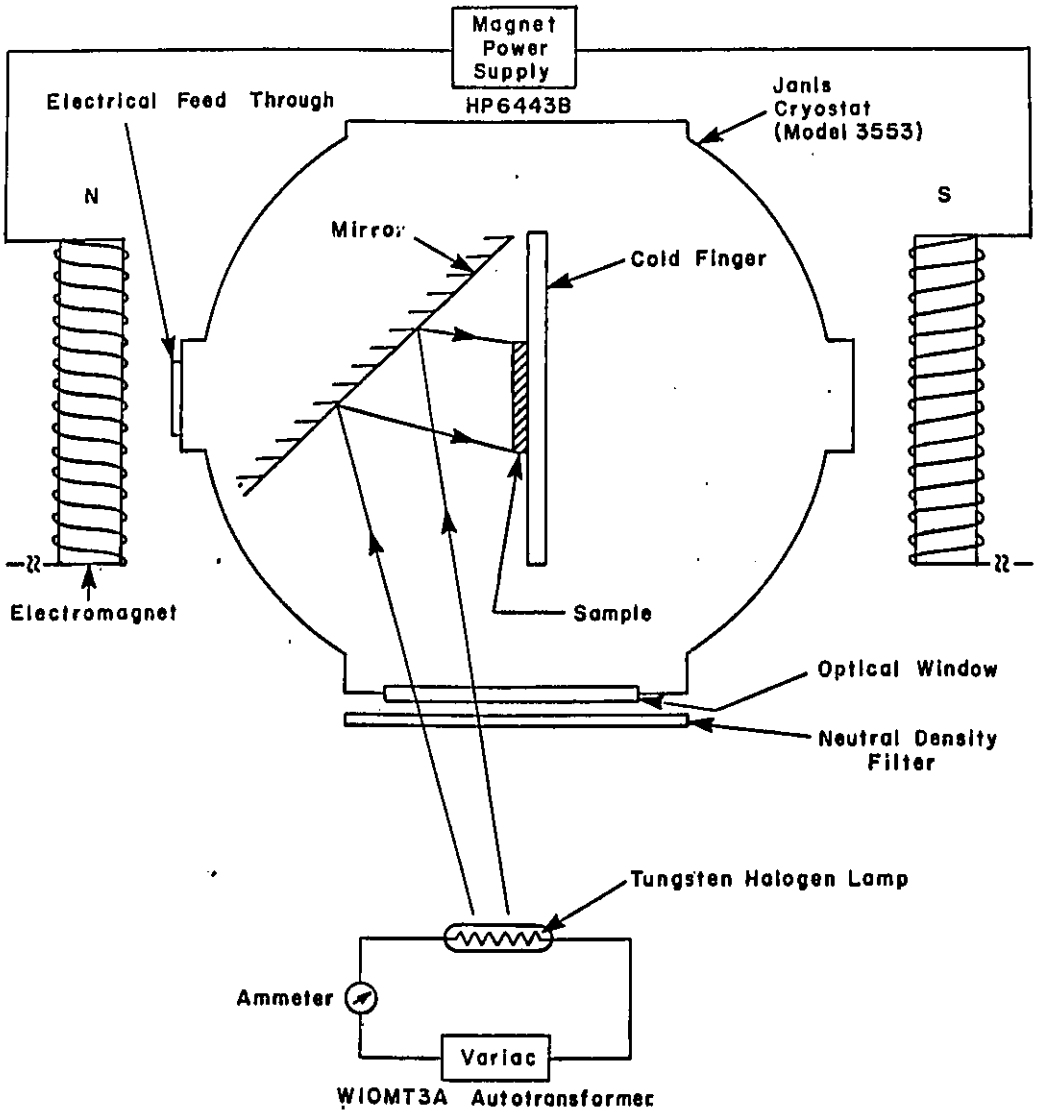

Figure 2.4: Schematic diagram of the experimental set-up for the Hall effect measurements

2.4 Hall Effect Measurement

The Hall effect measurements were done in the Vander Pauw geometry[35]. The circuit diagram for Hall effect measurements is shown in figure 2.3(a). For resistivity measurements, a current I_{12} was passed across the contacts 1 and 2, and the voltage V_{34} was measured across the contacts 3 and 4. The current I_{12} was measured in terms of a voltage across a standard resistor. Thus, I_{12} =voltage across the standard resistor/resistance of the standard resistor. The voltage across the standard resistor was measured in the voltage mode of the 617 Keithley electrometer. Similarly, a current I_{23} was passed across contacts 2 and 3 and the voltage V_{14} was measured across contacts 1 and 4. The resistivity of the sample was then calculated from

$$\rho = [\pi t_s / ln2][(R_1 + R_2)/2] f(R_1/R_2) ohm - cm \qquad (2.1)$$

where, f(R_1/R_2) is a function of the ratio R_1/R_2 and is nearly unity for $R_1 \approx R_2$, t_s is the sample thickness in cm and $R_1 = V_{34}/I_{12}$ and $R_2 = V_{14}/I_{23}$.

The Hall coefficient R_H was measured in the following manner: a current, I_{13}, was passed across the contacts 1 and 3; theoretically, there should be no voltage drop across contacts 2 and 4 (i.e. V_{24}=0) in the absence of a magnetic field assuming the sample was symmetrical. However, due to some asymmetry of the samples this voltage was not always zero. This voltage across 2 and 4 was suppressed with a counter balancing voltage supplied by the Keithley electrometer in the suppress mode. Then the forward magnetic field was smoothly ramped up to its desired value (to avoid voltage spikes through the sample) and the actual Hall voltage V_{24H_f} was measured on the electrometer. The magnetic field was then switched off. Again, the same current I_{13} was sent through the contacts 1 and 3

and the voltage developed across the contacts 2 and 4 was suppressed. The magnetic field direction was reversed and the magnetic field ramped up smoothly and the actual Hall voltage V_{24H_r} was noted from the electrometer. The entire measurement sequence was then repeated, but this time a current was passed across the contacts 2 and 4 and the voltage was measured across contacts 1 and 3. Using these measurements the Hall coefficient R_H was calculated from the expression

$$R_H = [V/I]_{av}[(t_s)/(H)]cm^3/C \tag{2.2}$$

where

$$(V/I)_{av} = 1/4[(V_{24H_f}/I_{13}) + (V_{24H_r}/I_{13}) + (V_{13H_f}/I_{24}) + (V_{13H_r}/I_{24})] \tag{2.3}$$

where V is in mV, I is in μA, t_s is the thickness of the sample in angstroms and H is the magnetic field in KG.

Knowing R_H, the carrier concentration and the carrier mobility were calculated from the expressions

$$n = 1/(R_H e)cm^{-3} \tag{2.4}$$

$$\mu_H = (R_H/\rho)cm^2V^{-1}s^{-1} \tag{2.5}$$

where $e = 1.602198 \times 10^{-19}C$.

Photo Hall effect measurements were performed in a similar manner in the same system with samples illuminated as described above.

2.5 Photoconductivity Measurement

For photoconductivity measurements, the resistance of the sample was measured in the V/I mode of resistance measurement at a fixed voltage with a Keithley 617

electrometer using the circuit of fig. 2.3(b). The model 617 Keithley electrometer has a built-in voltage source that can be used to make V/I resistance measurements. The voltage can be adjusted between -102.3 V and +102.4 V in 50 mV increments and has a maximum output current of 2 mA. The voltage source can be used in conjunction with the electrometer section of model 617 to measure resistances as high as 10^{16} Ω. In this mode, the measured resistance is automatically calculated from the applied voltage and the measured current in accordance with the standard formula: $R = V/I$. The measurements were carried out at different temperatures at fixed intervals from 77 K to 400 K. At each temperature the resistances were measured at different illumination intensities.

The dark resistance and resistance under illumination were measured at a fixed voltage. Then the dark and light currents were calculated from these resistance values. The photocurrent was calculated from the equation $I_{ph} = I_L - I_D$. Knowing photocurrent, the photoresistance could be calculated. The dark and the photo resistivity were calculated from the formula : $\rho = R * (t * l)/d$, where t is the thickness of the sample, l is the length of the sample between the contacts and d is the width of the sample. The thickness of the samples was determined using the stylus method. For all films deposited on glass, the thickness was measured using a Sloan Dektak II Stylus. The films were scratched by a razor blade, leaving a chasm whose depth was equal to the thickness of the films. The thickness of the films deposited on glass were assumed to be equal to the thickness of the films deposited under the same conditions on KBr or BaF_2. L and d were measured by a travelling microscope.

Structural and optical measurements on the CdTe and PbTe epilayers have been reported in previous publications[28,29,34] and also form the subject of a separate thesis[30].

2.6 Comment On Errors

Following were the probable errors involved in our measurements.

The error in temperature readings was $\approx \pm 1.5\%$, i.e., at 77 K the temperature reading was 77 ± 2 K and at 300 K it was 300 ± 5 K. The error in the resistivity values were $\approx \pm 6\%$, arising mainly from the thickness measurements of the samples, which has an accuracy of $\approx \pm 5\%$. The error in voltage and current measurements were very small. They were $\approx \pm 0.03\%$ and $\approx \pm 0.003\%$, respectively. The illumination intensity had an error of approximately $\prec \pm 1\%$ in the higher intensity region, and at the low intensities, the error was $\approx 1 - 2\%$. Error values in the Hall coefficient (eq.2.2) were $\approx \pm 7.5\%$, due to $\approx \pm 5\%$ error in thickness, $\approx \pm 1\%$ error in Hall voltage and $\approx \pm 1.5\%$ error in the magnetic field values. The values of carrier concentration (eq.2.4) and mobility (eq.2.5) had an error of $\approx \pm 8 - 10\%$ and $\approx \pm 13 - 15\%$, respectively.

Chapter 3

CdTe

3.1 Electrical Properties And Comparison With Other Methods

CdTe has been under extensive investigation for many years. Epitaxial thin films of CdTe have been deposited on different substrates by various techniques such as hot wall epitaxy[6], atomic layer epitaxy[8], molecular beam epitaxy [3-5], ionized cluster beam epitaxy[9], laser assisted deposition(LADA)[7], metelorganic chemical vapor deposition[41,42], photoassisted molecular beam epitaxy[11] and sputtering[28].

Schikora et al.[6] have used the hot wall epitaxy (HWE) method for the growth of high quality CdTe epitaxy on semi-insulating GaAs. The HWE CdTe films exhibit a resistivity of about 10^5 ohm-cm and show p-type conduction with a Hall mobility of about 100 $cm^2V^{-1}s^{-1}$ and carrier concentration of about

$3 \times 10^{12} cm^{-3}$ at 270 K.

Photo-assisted molecular beam epitaxy (PAMBE) has been used by Hwang et al.[11] to grow a series of undoped and doped CdTe films. The PAMBE-grown epilayers exhibit outstanding electrical properties as determined by Van der Pauw Hall effect measurements. This new film deposition technique differs from conventional MBE in that here the substrate is illuminated during the deposition process. The authors found that illumination during the film deposition process had a pronounced effect on the electrical properties. The mobility increases with decreasing temperature, consistent with phonon limited behavior, and reaches a maximum value of 6600 $cm^2V^{-1}s^{-1}$ at 30 K. This is the highest electron mobility for CdTe thin films reported so far. The carrier concentration is essentially constant in their case at $\approx (2-4) \times 10^{15} cm^{-3}$. It then decreases with decreasing temperature to a value of $\approx 2 \times 10^{14} cm^{-3}$ at 20 K.

Yoshiji Kawai et al.[10] studied the dependence of dark conductivity on temperature for (111) oriented CdTe films evaporated on glass. Two activation energies were observed in the extrinsic conduction region. The activation energy in the intrinsic region was 0.59 eV, while for extrinsic conduction, in the low temperature region the activation was 0.027 eV and in the high temperature region the activation energy was 0.055 eV. The value of 0.027 eV is close to 0.02 eV, which is the activation energy of native donors due to the interstitial excess cadmium.

Takaoka et al.[36] studied the photovoltaic behavior of CdTe films. A Xe lamp of 100 mW/cm^2 was used as the light source. The current- voltage characteristic was measured to study the electrical properties of CdTe films. Photoconductivity was found to be about $10^{-9}(\Omega cm)^{-1}$ and was larger by a factor of 100 than the dark conductivity. Table 3.1 gives the electrical properties of CdTe epilayers grown by different techniques.

Not many groups have performed detailed Hall effect electrical measurements of epitaxial CdTe thin films because of difficulties associated with Hall effect measurements on high resistivity samples and because of the higher conductivity of the substrates (usually GaAs) used for heteroepitaxial growth. The growth of heteroepitaxial layers of CdTe on insulating KBr by sputter-deposition at NRC has allowed the direct measurement of electrical properties of the epilayers without interference from the substrate. In this Chapter we present the results of photoconductivity and Hall effect measurements on sputter-deposited (100) CdTe || (100) KBr epilayers.

3.2 Results

The structural properties of sputter-deposited CdTe epilayers have been reported previously[28,34]. These were the first report of the epitaxial growth of CdTe films by sputter-deposition. For the growth conditions mentioned in Chapter 2 (section 2.1), epitaxial growth of (100) CdTe || (100) KBr was observed.

Technique Used	Mobility $cm^2V^{-1}s^{-1}$	Carrier concentration cm^{-3}	Resistivity $\Omega - cm$	Reference
Hot Wall Epitaxy	100	3×10^{12}	$\approx 10^5$	6
MBE	900	-	2×10^7	42
Photo assisted MBE	$770_{(R.T.)}$	$2\text{-}4\times10^{15}$	-	11
	$6600_{(30K)}$	$2\times10^{14}_{(20K)}$	-	

Table 3.1: Electrical properties of epitaxial CdTe thin films

Figure 3.1 is a plot of a typical current-voltage (I-V) characteristics of CdTe samples with gold contacts. The linear nature of the I-V curve shows that the Au contacts were ohmic. All subsequent measurements reported were made with Au contacts. In this section we have given results for one particular sample (SRD 8) which is typical of the sputter-deposited epitaxial CdTe samples. The conductivity measurements of the epitaxial CdTe samples were undertaken in the temperature range of 77 K to 400 K. The Hall effect measurements were not possible at lower temperatures because of the high resistivity of the samples; therefore, dark Hall effect measurements were made only in the high temperature range (320 to 400 K) while the Hall effect measurements under illumination were performed in the temperature range of 140 to 400 K.

The temperature dependence of dark conductivity and photoconductivity

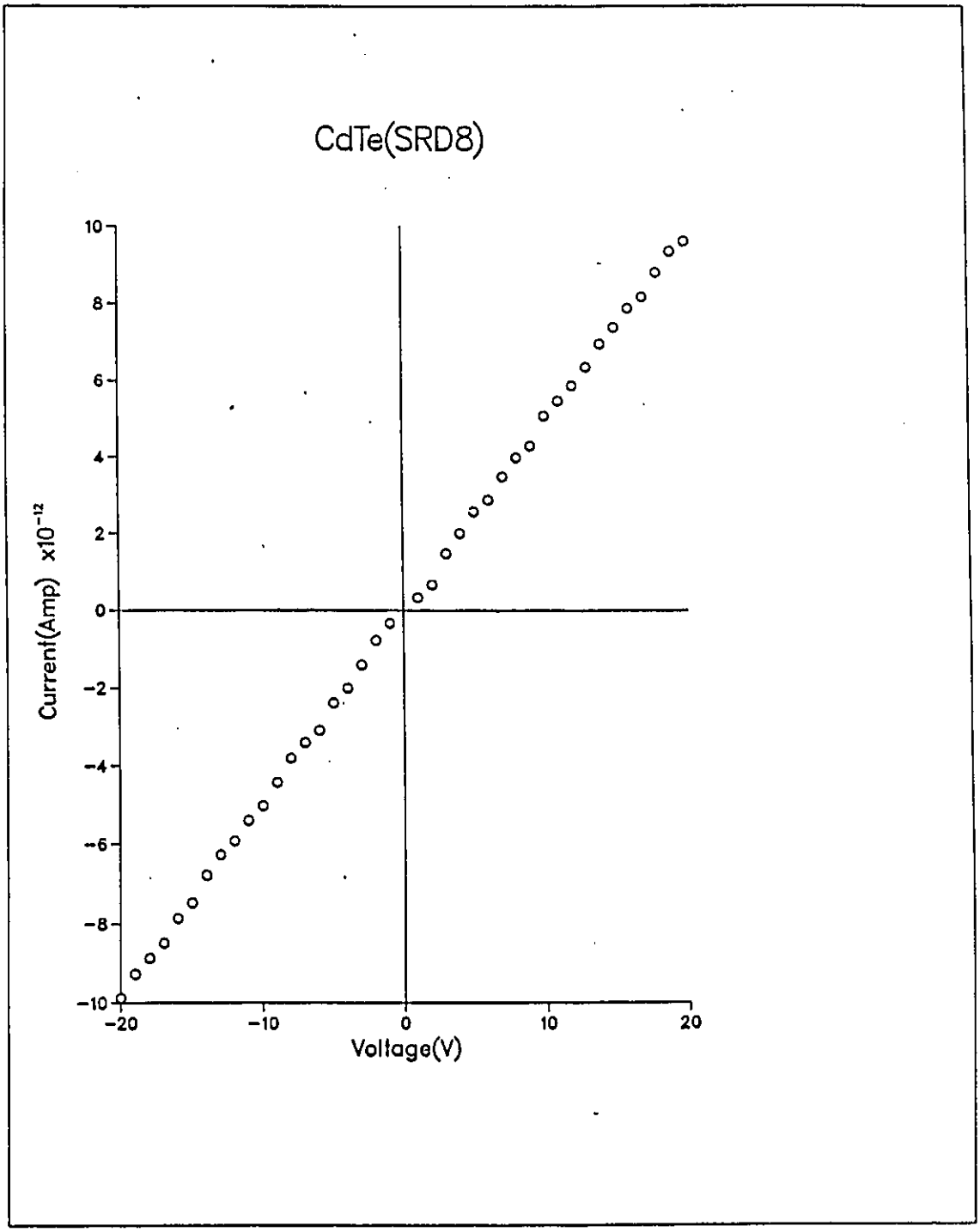

Figure 3.1: I-V characteristics of a CdTe epilayer with Au contacts

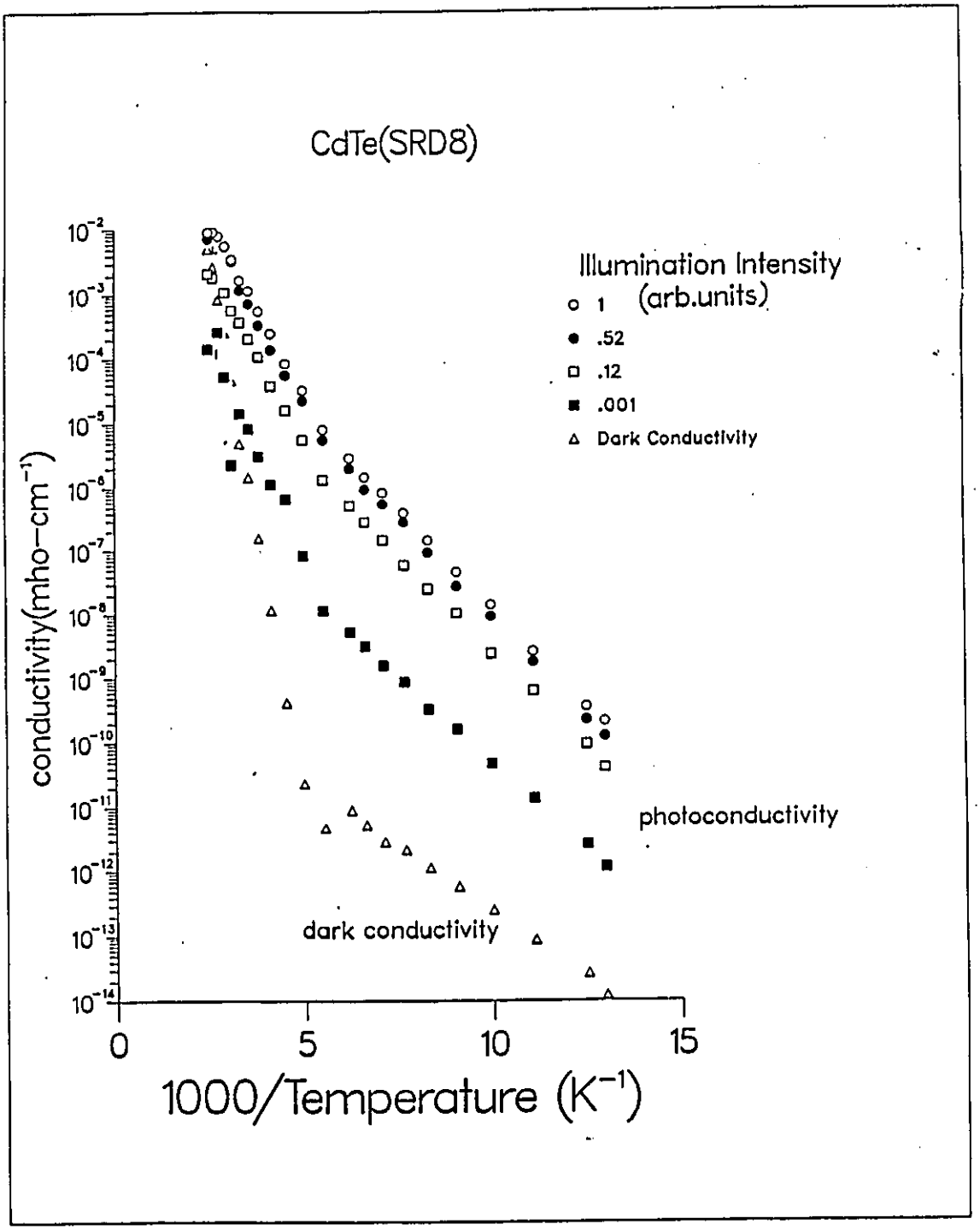

Figure 3.2: Temperature dependence of conductivity under various illumination levels

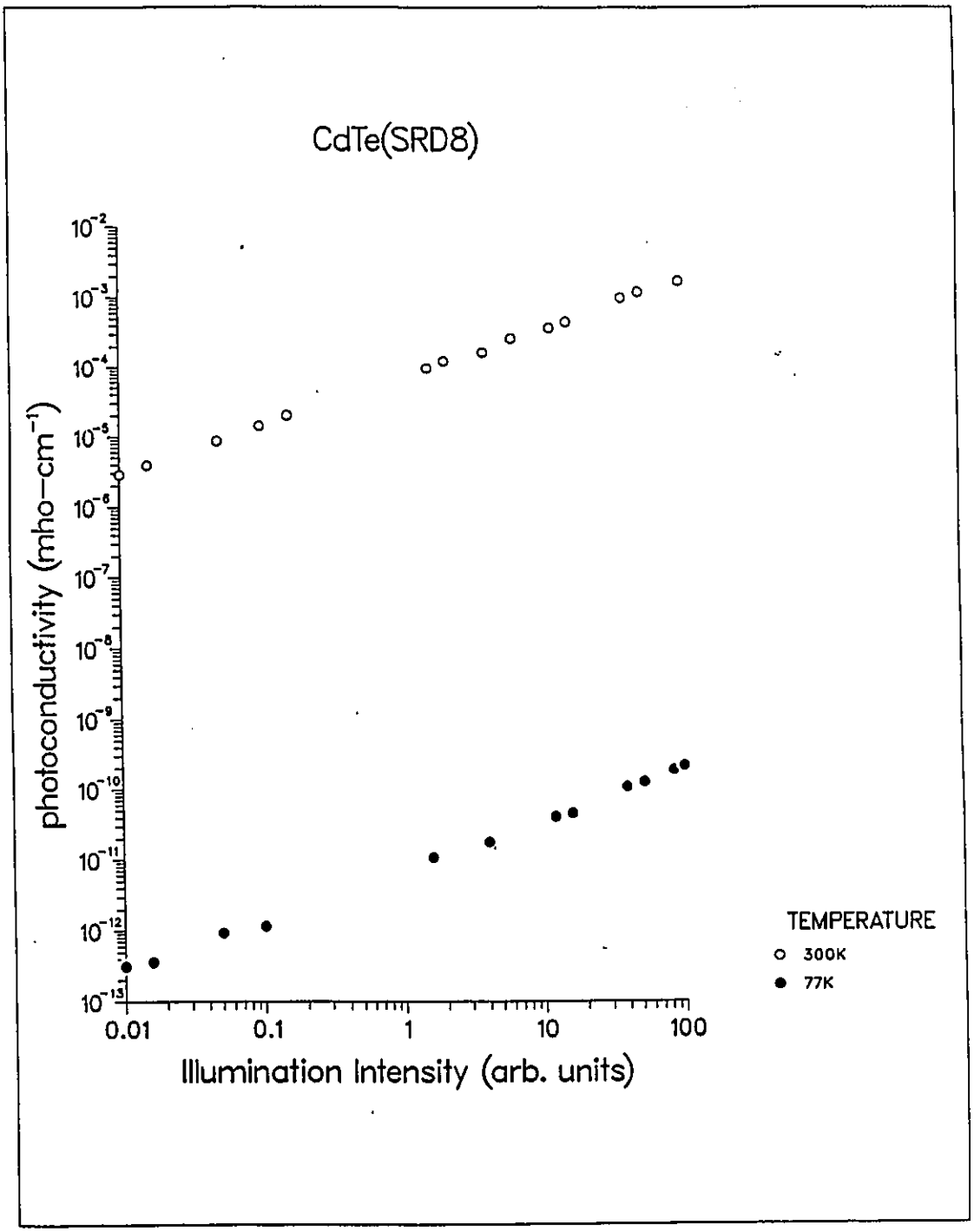

Figure 3.3: Intensity dependence of photoconductivity for two different temperatures

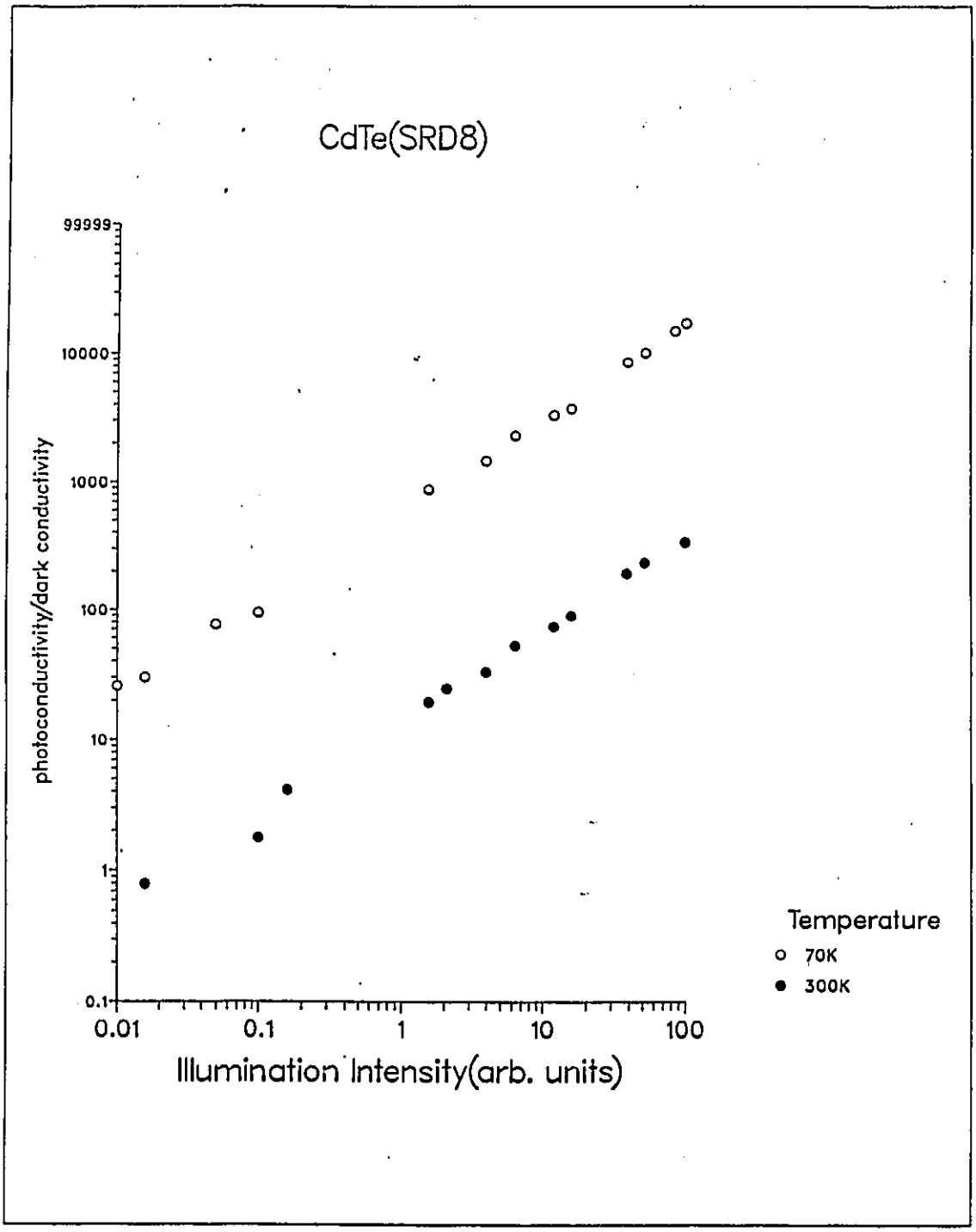

Figure 3.4: $\sigma_{ph}/\sigma_{dark}$ as a function of illumination intensity

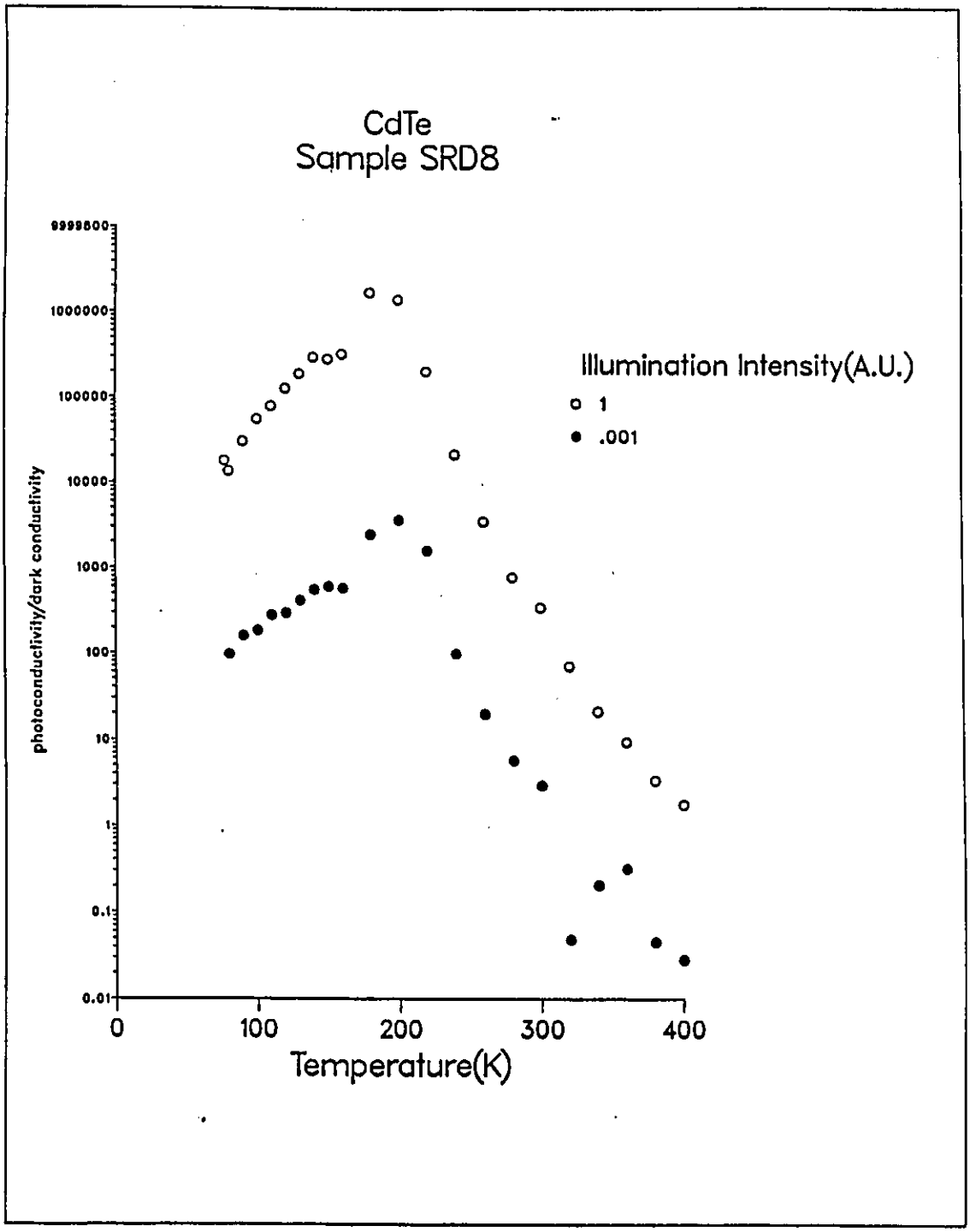

Figure 3.5: $\sigma_{ph}/\sigma_{dark}$ as a function of temperature

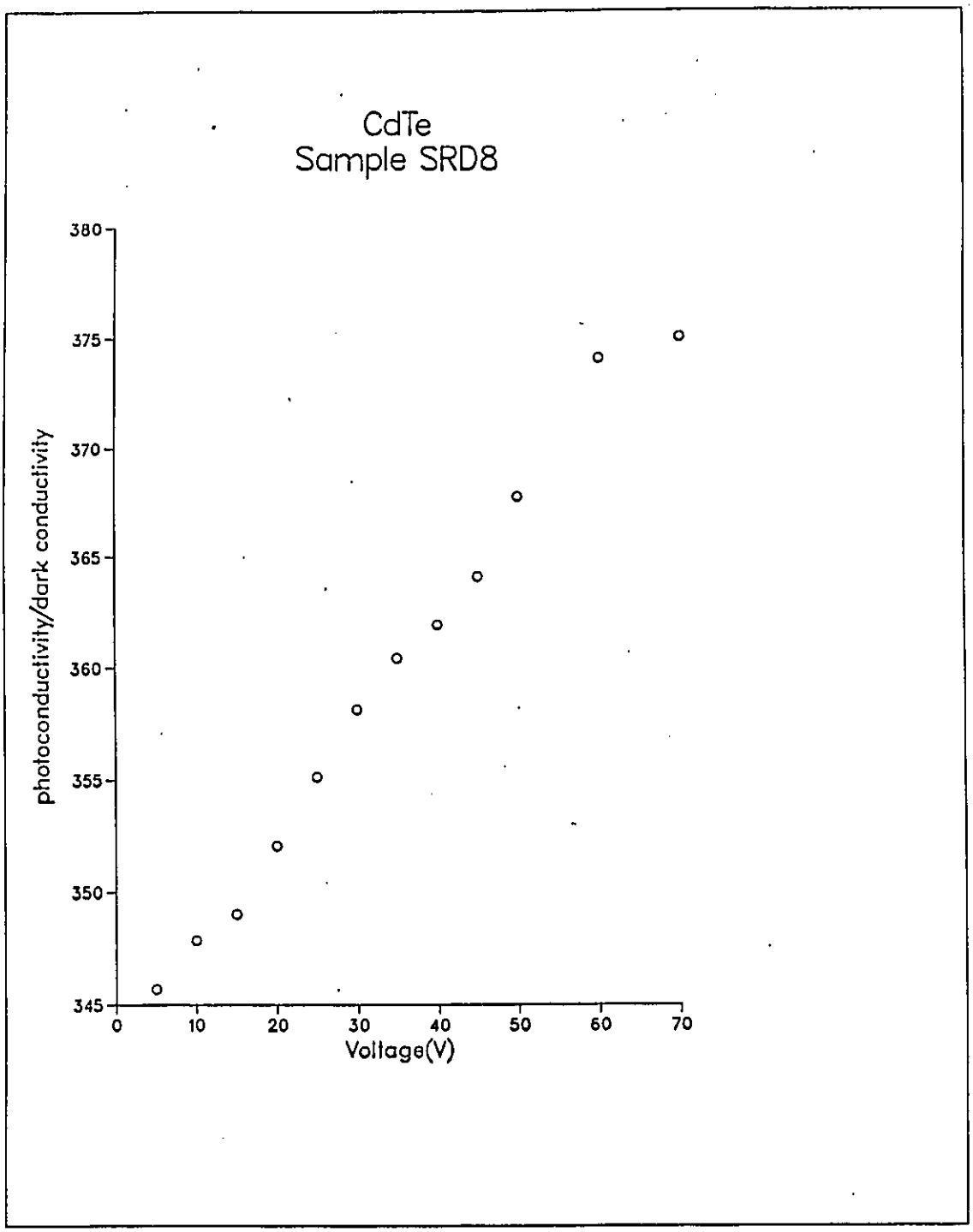

Figure 3.6: Dependence of $\sigma_{ph}/\sigma_{dark}$ on voltage

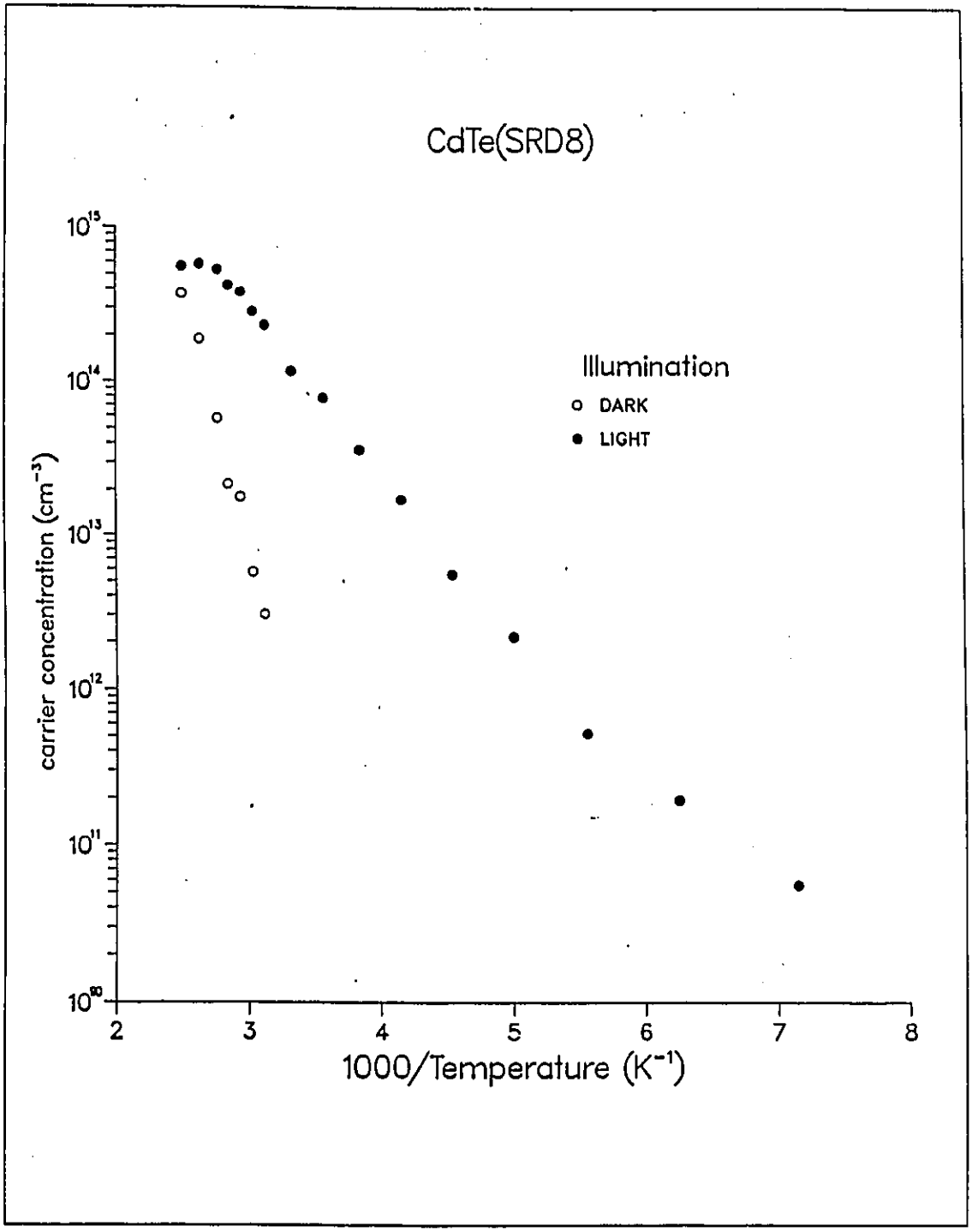

Figure 3.7: Dependence of carrier concentration in dark and under illumination on temperature

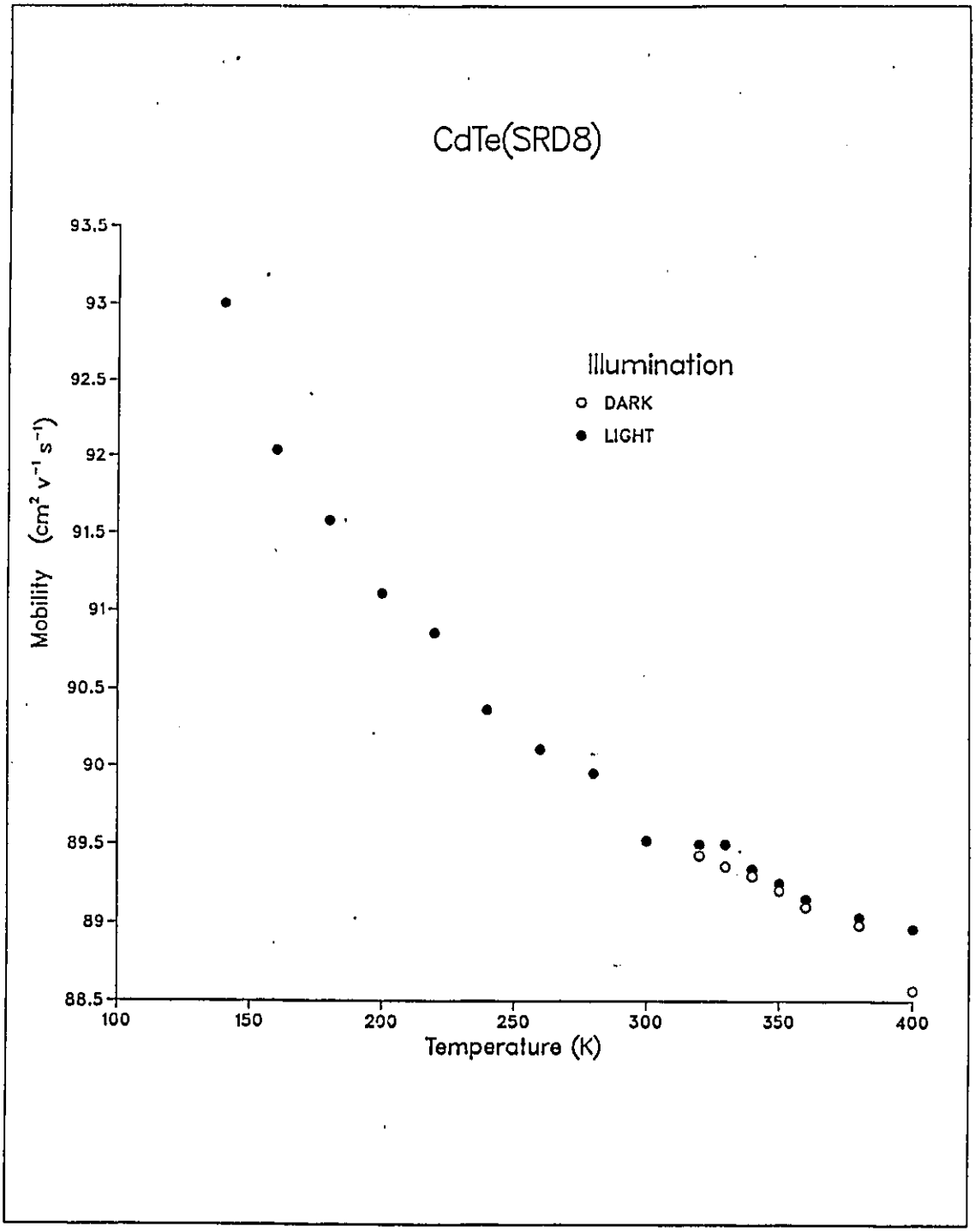

Figure 3.8: Temperature dependence of Hall mobility in dark and under illumination

under various illumination levels is shown in figure 3.2. Both the dark conductivity and photoconductivity at all intensities exhibit a thermally activated behavior. The Arrhenius plot (fig. 3.2) shows a break both for dark conductivity and photoconductivity, indicating two regions with different activation energies. Also, the photoconductivity curves at all intensity levels are essentially parallel and shifted to higher values with increasing illumination intensity. We can see from the plot that at higher temperatures there is a cross-over between the dark conductivity and the photoconductivity and this cross-over point moves to higher temperatures at higher illumination intensities. Also the photoconductivity tends to attain a maximum value at the higher temperature range.

Figure 3.3 shows the intensity dependence of photoconductivity (σ_{ph}) at two different temperatures. It was observed that the photoconductivity was proportional to the illumination intensity: $\sigma_{ph} \alpha f^{\gamma}$. The values of γ as calculated from the slopes of the plots in fig. 3.3 are 0.67 at 300 K and 0.72 at 77K.

The ratio $\sigma_{ph}/\sigma_{dark}$ as a function of illumination intensity for two different temperatures is shown in fig. 3.4. The slopes of the plots at 300 K and 77 K give the values 0.6 and 0.76, respectively.

Figure 3.5 shows the plot of the ratio $\sigma_{ph}/\sigma_{dark}$ as a function of temperature. This ratio reaches a maximum at about 200 K. Also on the lower temperature side of the maximum, the change of the ratio is gradual while on the higher temperature side of the maximum, the ratio decreases rapidly.

The dependence of $\sigma_{ph}/\sigma_{dark}$ on voltage at room temperature is shown in figure 3.6. From the figure we can see that the ratio $\sigma_{ph}/\sigma_{dark}$ increases approximately linearly with voltage.

Figure 3.7 shows the dependence of carrier concentration in dark and under illumination on temperature. The Hall coefficient was found to be positive for all

the CdTe samples both in dark and under illumination.

The temperature dependence of Hall mobility in dark and under illumination is plotted in figure 3.8. It was found that the mobility had a very weak dependence on temperature. Also, illumination had no effect on carrier mobility. The photoconductivity is, therefore, due to a change in carrier concentration and not due to a change in carrier mobility, as expected for epitaxial films.

3.3 Discussion

Au contacts are known to be ohmic for p-type CdTe[40]. The observation of ohmic behavior of the sputter-deposited CdTe samples with Au contacts is consistent with the p-type conductivity deduced from the positive sign of the Hall coefficient observed in the samples.

The dark carrier concentration(Fig. 3.7) is thermally activated. To determine the activation energy the carrier concentration data was fitted to the equation

$$p(N_d + p)/(N_a - N_d - p) = (N_v/g)[exp(-E_{A1}/kT)] \qquad (3.1)$$

where p is the measured carrier(hole) density, N_d is the density of donor levels, N_a is the density of acceptor levels, N_v is the density of states at the top of the valence band, g is the degeneracy and E_{A1} is the activation energy which corresponds to the position of the acceptor level. N_v is given by $2(2\pi m^*_{dh} kT/h^2)^{3/2}$. A plot of (carrier concentration$\times T^{-3/2}$) versus 1000/T is shown in Fig. 3.9. The value of E_{A1} determined from the fit is 0.64 eV, using g=4 and m^*_{dh}=0.82 m_0.

To analyze the photoconductivity and photo-Hall effect data, it is first necessary to choose a proper model. The observed temperature and intensity dependences of photoconductivity for our samples are qualitatively similar to those observed in some amorphous chalcogenides[45,46] and amorphous Si[47,48,49]. Simons and Taylor[45,46] have developed a theory of photoconductivity to explain the observed photoconductivity behavior in the various temperature and illumination regimes in p-type amorphous semiconductors. Our data appears to be best described by their model of two traps, E_1 one in the upper-half of the bandgap and E_2 in the lower-half and a Fermi-level(in dark) located at an energy E_{f_0} situated in the lower-half of the bandgap, in accordance with the fact that the material is p-type. The positions of the quasi-Fermi levels E_{fn} and E_{fp} under illumination is determined by the level of illumination and the temperature. Remembering that the photocurrent is carried by holes (since the Hall coefficient under illumination is positive), the expression for the density of photocarriers Δp is given by

$$\Delta p = [fN_v/(vS_pN_t)]^{1/2} exp[-(E_2 - E_v)/2kT] \qquad (3.2)$$

where N_t is the trap density, f is the illumination intensity, v is a thermal velocity and S_p is the capture cross-section of the trap for holes. The above expression is valid for moderate illumination levels when $E_1 \succ E_{fn}$ and $E_2 \prec E_{fp}$ or for intermediate illumination levels (higher than moderate) assuming $E_c - E_1 \succ E_2 - E_v$. Our data, of course, does not allow us to distinguish between the two cases. We should point out another important assumption made in deriving the above expression, namely, the light is absorbed uniformly throughout the depth of the sample.

Figure 3.10 shows a plot of $n_L T^{-1/2}$ versus 1000/T where n_L is the measured carrier concentration under illumination at the highest illumination level. From the slopes of the two linear regions two hole trap levels were determined : $E_2(1)$=0.36 eV and $E_2(2)$=0.23 eV. Fig. 3.11 shows a similar plot for $(\sigma_{ph}T^{-1/2})$

versus 1000/T. The trap levels calculated from Fig. 3.11 are $E_2(1)$=0.40 eV and $E_2(2)$=0.23 eV. The values of $E_2(2)$ from the two measurements are in excellent agreement. The slight difference in the values of the $E_2(1)$ level determined from the Hall effect and photoconductivity measurements may be due to the fact that n_L is the carrier concentration measured under illumination whereas σ_{ph} is the excess conductivity under illumination. At the higher temperature range where the dark conductivity (dark carrier concentration) is large and comparable to the photoconductivity (photo-carriers), n_L is not equal to Δn, where Δn is the excess photocarrier($\Delta n = n_L - n_{dark}$) density.

According to the above expression (eq.3.2), the photoconductivity should vary with intensity with a power(γ) of 1/2. However, our data shows that $0.5 \prec \gamma \prec 1.0$. The model given by Rose[33] of an exponential distribution of traps to explain γ values between 0.5 and 1.0 does not apply in our case for the following reasons : (a) we observe an exponential dependence of σ_{ph} on T^{-1} whereas the model of Rose predicts a temperature dependence of the form $\sigma_{ph} \alpha N_c^{T/(T+T_1)}$ where $\gamma = T_1(T + T_1)$ and (b) the values of T_1 obtained from the intensity dependence of σ_{ph} at 77 K and 300 K (Fig. 3.3) are very different. One plausible explanation for a γ value between 0.5 and 1.0 is that, in the temperature range over which the measurements were carried out, some other trapping mechanism with an intensity dependence of unity was also operative. The model of Simmons and Taylor predicts a linear dependence of photoconductivity on intensity at very low levels of illumination. Since CdTe is strongly absorbing with a high absorption coefficient above the bandgap, it is entirely reasonable to expect that the sample is not uniformly illuminated along the thickness of the layers and, therefore, regions of low illumination are always present in the bulk of the layers away from the illuminated surface.

The temperature dependence of the dark conductivity could be fitted with a sum of two-exponentials:

$$\sigma_{dark} = \sigma_1 + \sigma_2 = \sigma_{01} exp(-E_{D1}/kT) + \sigma_{02} exp(-E_{D2}/kT) \qquad (3.3)$$

where E_{D1} and E_{D2} are the thermal activation energies for two different processes, one predominant in the high-temperature and the other in the low-temperature region, respectively. Since $\sigma = pe\mu_p$ (the sample is p-type) the pre-exponential terms in the equation for σ_{dark} would have the form $\sigma_{01} = N_{v1}(T)e\mu_p(T)$. Hall effect measurements show that the mobility is very weakly temperature dependent. Neglecting the temperature dependence of the mobility one can plot ($\ln \sigma_{dark} T^{-3/2}$) versus 1/T (Fig. 3.12) and obtain the following values for the activation energies: E_{D1}=0.62 eV, E_{D2}=0.07 eV. For an essentially temperature independent mobility, the thermally activated dark conductivity behavior could be explained by the activation processes controlling the carrier concentration; therefore, the activation energies determined for the dark conductivity should be the same as that determined for the dark carrier concentration. This is indeed found to be the case.

Photoluminescence measurements, reported previously[30], indicate that the origin of the deep acceptor level at 0.64 eV is due to deviation from stoichiometry. The level can be attributed to cadmium vacancies[1]. Other workers[1] have observed acceptor levels between 0.05 and 0.20 eV and have attributed the levels to cadmium vacancies, cadmium vacancy-complexes or native defects. The acceptor level at 0.08 eV in our samples can also be assigned to any of the above. Photoluminescence studies also indicate strong evidence for recombination centers originating at or from structural defects such as dislocations. We attribute the trap levels determined from photoconductivity measurements at $\approx$ 0.4 eV and $\approx$ 0.2 eV above the valence band to structural defects such as dislocations, twins and stacking faults present in the epilayers.

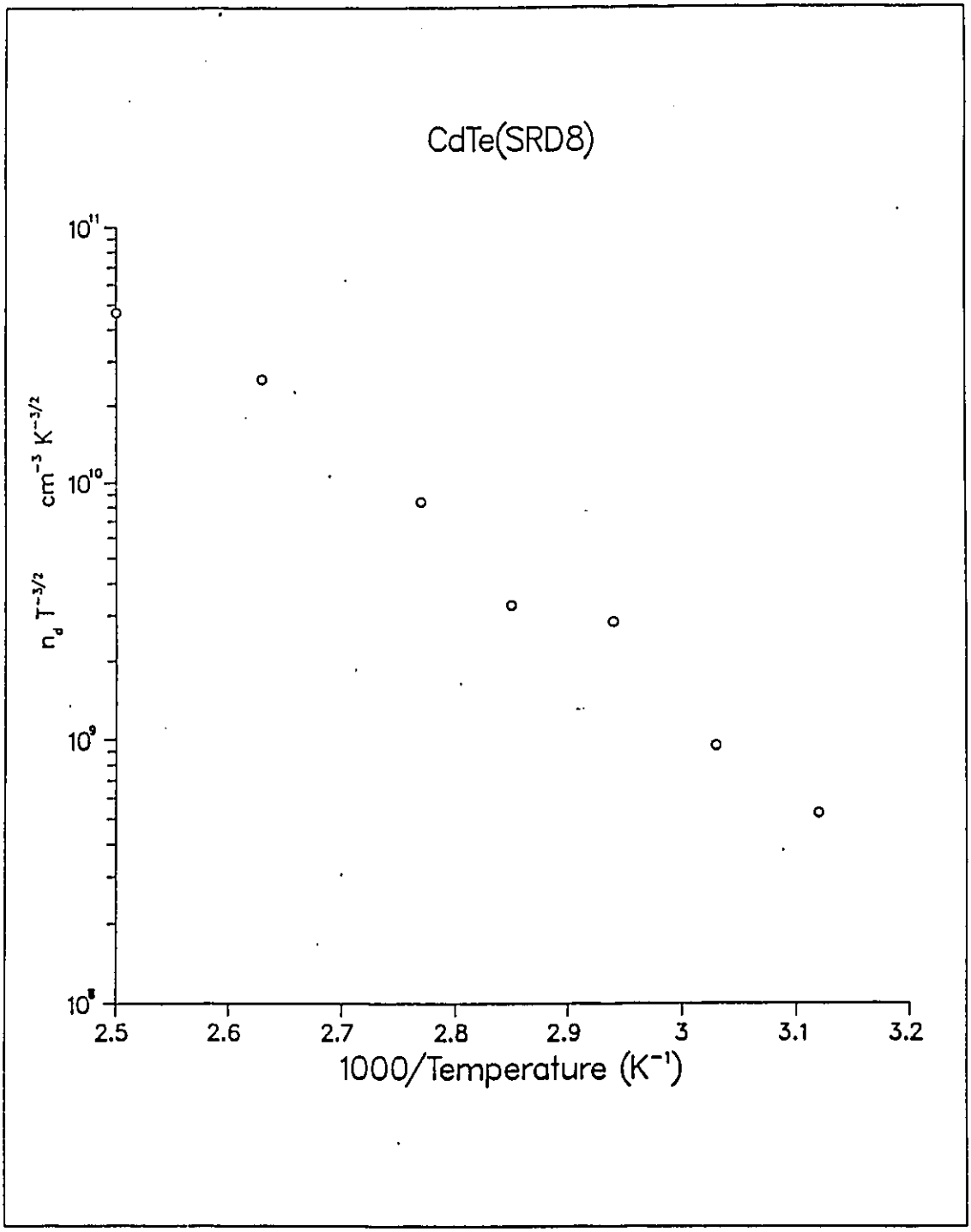

Figure 3.9: $n_{dark} \times T^{-3/2}$ vs 1000/T

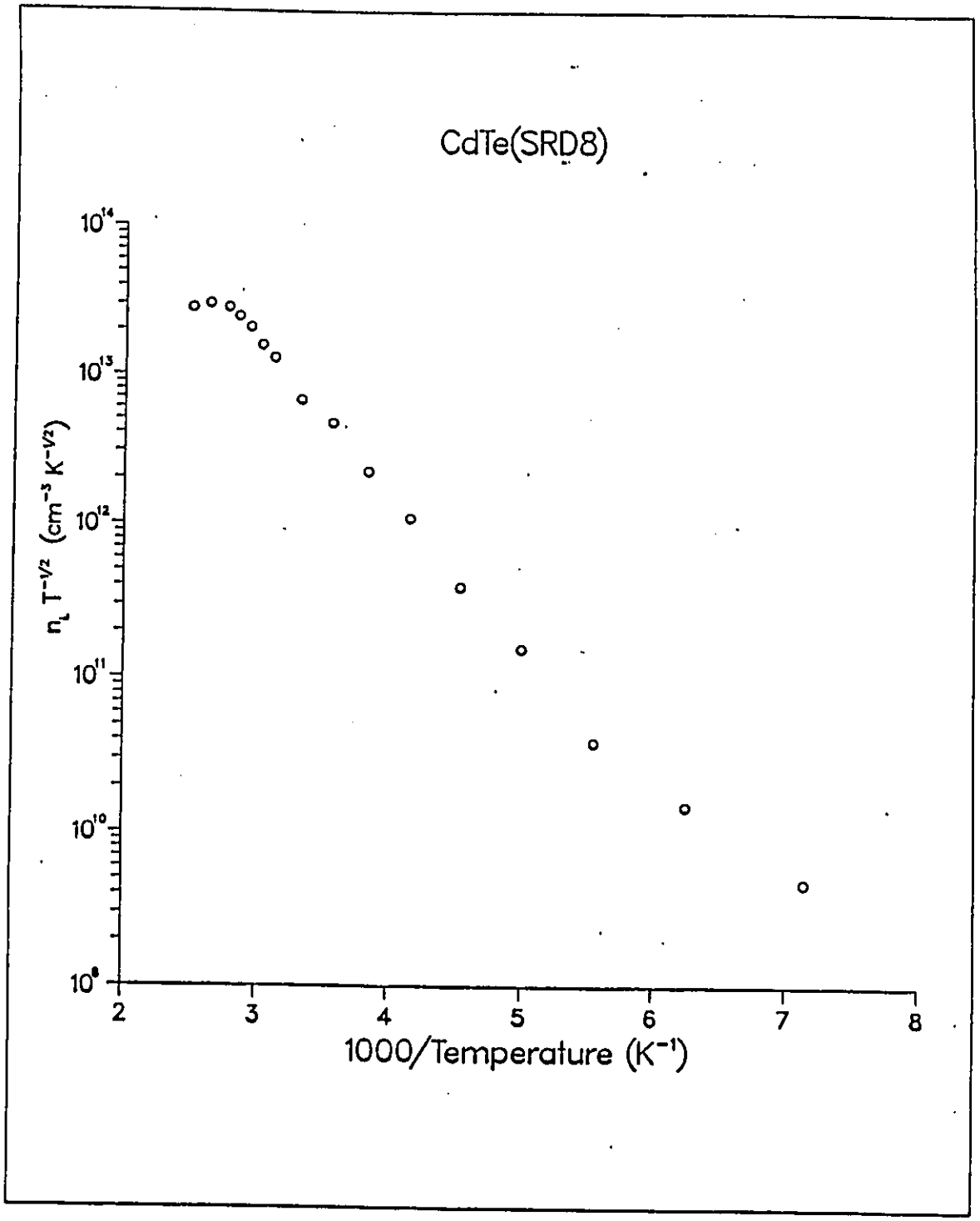

Figure 3.10: $n_L \times T^{-1/2}$ vs 1000/T

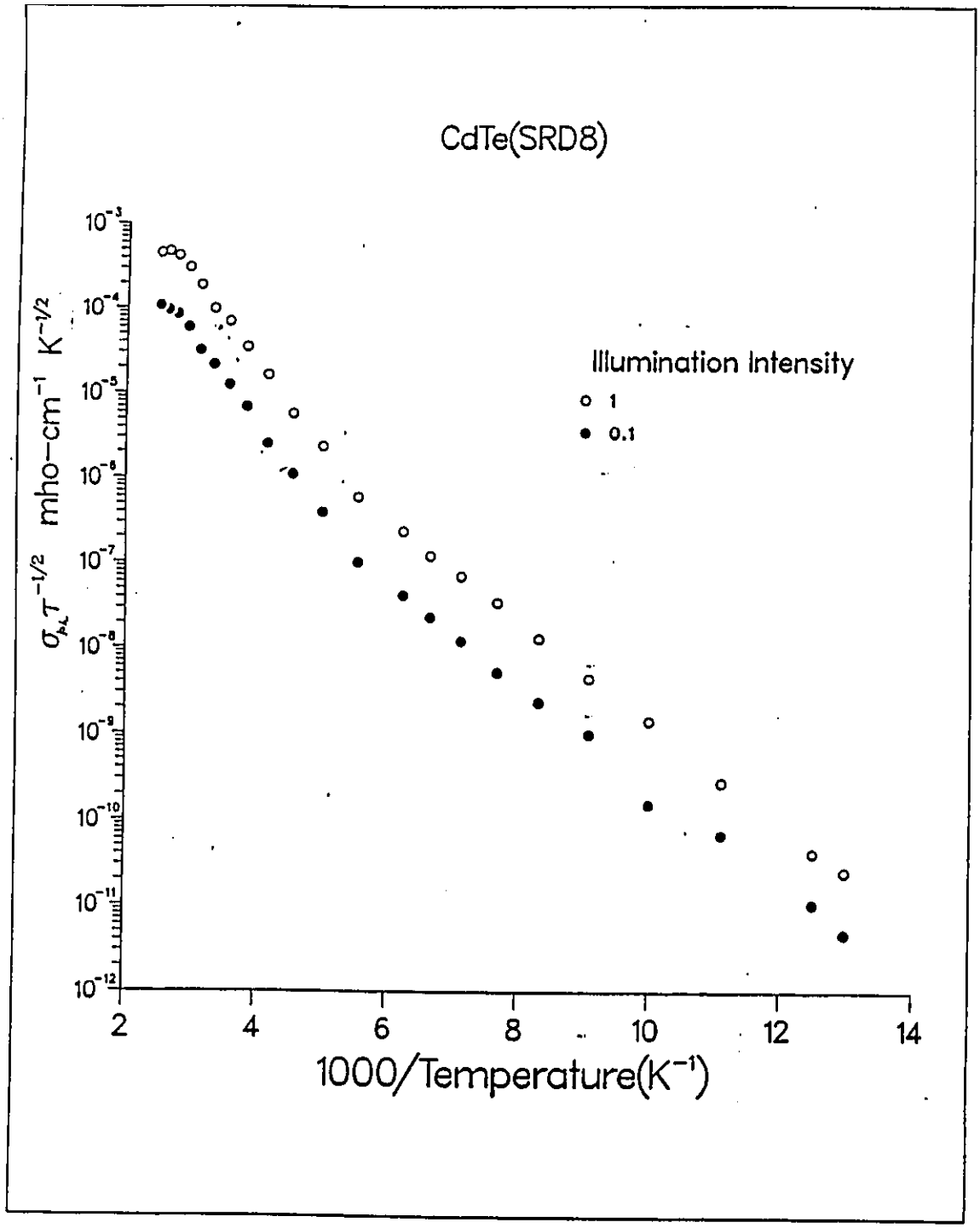

Figure 3.11: $\sigma_{ph} \times T^{-1/2}$ vs 1000/T

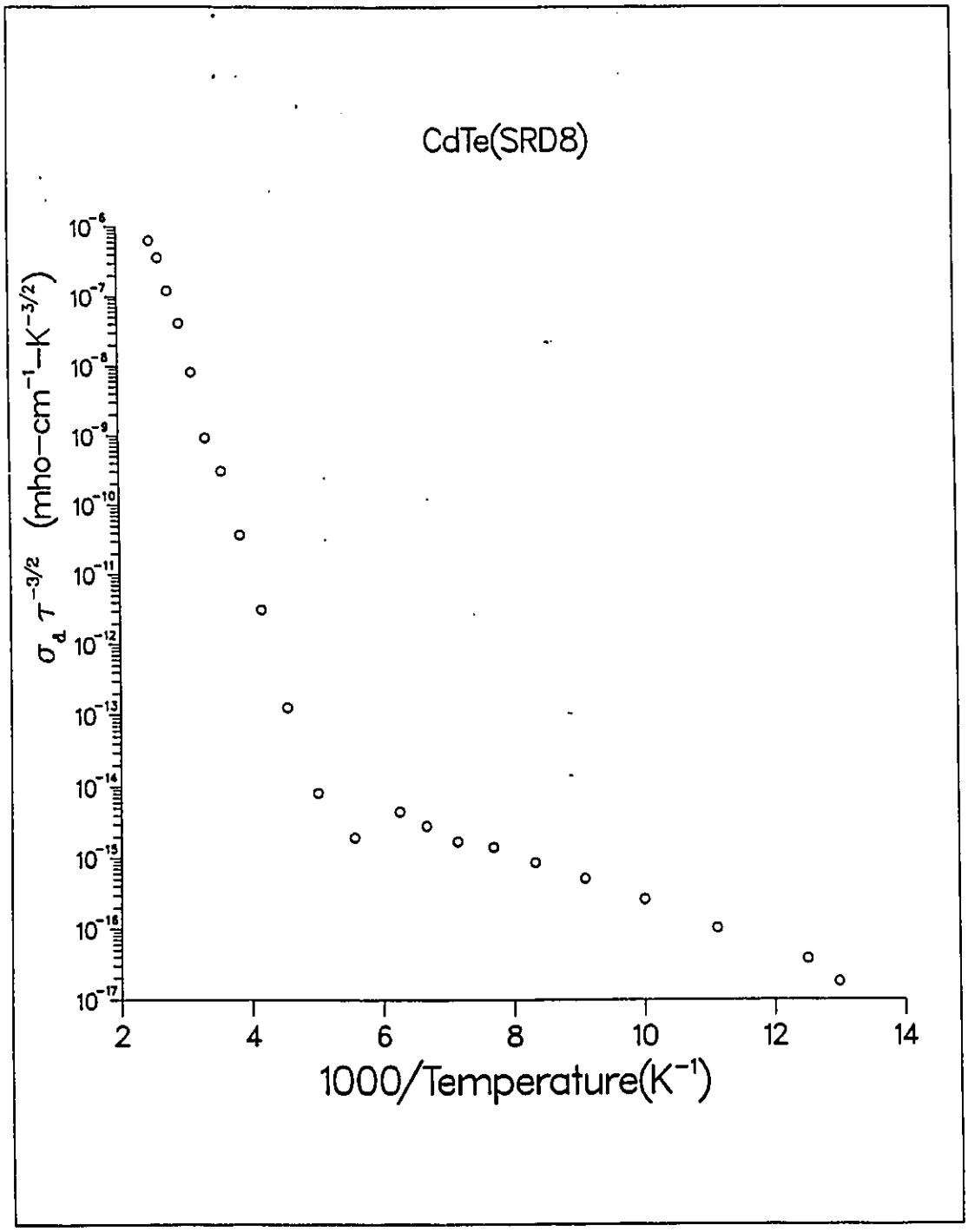

Figure 3.12: $\sigma_{dark} \times T^{-3/2}$ vs 1000/T

3.4 Conclusion

Sputter-deposited heteroepitaxial layers of (100) CdTe ‖ (100) KBr prepared at growth temperatures of 300-325 ^0C are found to be p-type with high dark resistivities on the order $\approx 2 \times 10^5$ ohm-cm. The epilayers are highly photoconducting and exhibit photoconductivity to dark conductivity ratios as high as $\approx 1.6 \times 10^6$ at around 180 K. The photoconductivity is observed to exhibit a sublinear dependence on intensity. Photo-Hall effect measurements show that the photoconductivity is due to change in carrier concentration and not due to any enhancement in the carrier mobility. Moreover, the photocurrent is carried by holes. From the temperature dependence of the dark conductivity, acceptor levels have been determined at 0.64 eV and 0.08 eV above the valence band. Hole trap levels at ≈ 0.4 eV and ≈ 0.2 eV above the valence band have been determined from the temperature dependence of the photoconductivity.

Chapter 4

Hall Measurements On PbTe Epilayers

4.1 Introduction

The structural properties of the sputter-deposited PbTe epilayers prepared on BaF_2 under systematically varied growth conditions have been reported previously[29]. The results are summarized in fig. 4.1 [taken from ref(29)] which is a plot of Γ versus growth rate , where the parameter Γ is the ratio of the diffraction intensity I_{222} for the (222) orientation to that of the total diffraction intensity $[I_{200}+I_{220}+I_{222}]$ and is a measure of the quality of the epitaxial growth of PbTe on (111) BaF_2. A

Γ value of unity indicates single crystal, epitaxial growth of (111) PbTe parallel to (111) BaF_2. It was found that the layers grown at a low substrate temperature ($\approx 180^0$C) without a substrate bias at all growth rates, were polycrystalline and randomly oriented. However, at 180 ^{0}C on application of a substrate bias of -10 V, epitaxial films were obtained at all deposition rates. At 260 ^{0}C, it was found that epitaxial films could be grown with or without substrate bias at all deposition rates. Also, at the lower substrate temperature (180-260 ^{0}C) some weak diffraction peaks were observed which could be identified as being due to free tellurium. At higher substrate temperatures (330- 410 ^{0}C), without substrate bias, (111) epitaxy was obtained only at lower deposition rates. But with a -10 V substrate bias, epitaxial growth was observed at all growth rates up to 2.0 μ/h. At the high growth temperatures, weak X-ray diffraction peaks due to free Pb were observed. The epitaxial growth at 260 ^{0}C without substrate bias led to the hypothesis in ref.(29) that at 260^{0}C, stoichiometric growth was obtained which favoured (111) epitaxy. Films grown at higher temperatures (330-410 ^{0}C) and lower temperatures(180 ^{0}C) were thought to be non-stoichiometric which required the application of a substrate bias for epitaxial growth. It was suggested that the films with excess Pb (grown at 330 and 410 ^{0}C) were n-type and those with excess Te (grown at 180 ^{0}C) were p-type. Hall effect measurements were, therefore, undertaken on epilayers grown at different substrate temperatures to test and confirm the hypothesis put forward in ref(29).

In addition, measurements of Hall mobility and temperature dependence thereof were also made on these samples to determine scattering mechanisms responsible for limiting the mobility values in these sputter-deposited layers and for comparison with values obtained on PbTe epilayers grown by other techniques.

Before proceeding to the next section reporting our results, we first summa-

rize the salient electrical properties reported in literature of PbTe epilayers grown by other workers.

Holloway and Logothetis[36] studied high mobility epitaxial layers of PbTe on BaF_2 substrate grown by MBE followed by post-growth annealing. They found that the Hall mobility remains typical of good bulk crystals in the range 300-50 K. They found a strong dependence of mobility and carrier concentration on annealing. Mobility increased drastically with annealing. In the range 300 - 50 K the Hall mobilities varied as T^c with c=-5/2. Such behavior is typical of good bulk crystals. Below 50 K the Hall mobilities tended to saturate. Such behavior was interpreted as a consequence of the carrier mean-free-path being limited by the size of the subgrains that comprised the epitaxial layer.

P.R.Vaya et al.[12] studied the thickness dependence of Hall mobility of hot-wall epitaxy (HWE) grown epitaxial PbTe films. It was observed that the mobility very strongly depends on thickness for thin films but becomes independent of film thickness beyond 5 μm, approaching bulk value. The constant value of the Hall coefficient in the temperature range 77 to 300 K showed the extrinsic nature of these films. The carrier concentration $\approx 10^{18} cm^{-3}$ was attributed to deviation from stoichiometry. The Hall mobility was found to increase with decreasing temperature. It was observed that films having thickness equal to or more than 5 μm followed a $T^{-2.3}$ law which was in good agreement with the theoretically predicted $T^{-2.33}$ law for bulk- like films. It was also noted that the rate of increase of mobility with decreasing temperature became slower as the thickness of the film decreased. This showed that the contribution of a surface dependent scattering process in limiting the mobility was more significant for thinner films. A. Lopez-Otero [25] prepared epitaxial PbTe films on (111)BaF_2 substrates using a vacuum evaporation method. The PbTe films had mobilities as large as $2.5 \times 10^6 cm^2 V^{-1} s^{-1}$ at 13 K. In the

range of 300-35 K, the Hall mobility curves had a slope in the neighbourhood of -5/2. The mobility value tend to saturate below 35 K. In table 4.1 some of the electrical properties of PbTe films grown by different techniques are given.

4.2 Results

Two I-V characteristics, typical of r.f. magnetron sputter-deposited PbTe films, are given in figures 4.2 and 4.3. It was found that PbTe epilayers deposited at 180 ^{0}C and 260 ^{0}C (with or without substrate bias) exhibited linear I-V behavior with evaporated Au contacts (fig. 4.2), whereas samples deposited at 330 ^{0}C and 410 ^{0}C (again with or without bias) exhibited linear I-V characteristics with evaporated In contacts (fig. 4.3). The above results suggested that Au formed ohmic contacts to PbTe samples deposited at 180 ^{0}C and 260 ^{0}C whereas In formed ohmic contacts to samples prepared at the higher growth temperatures. Gold is known to form ohmic contacts to p-type PbTe[16] and In is known to give ohmic behavior with n-type PbTe[43]. Thus measurements of the I-V characteristics provided the first indication of the dependence of the conductivity type of the PbTe epilayers on deposition temperature. More direct evidence of the n- and p-type nature of the PbTe samples was obtained from the Hall measurements. Tables 4.2, 4.3 and 4.4 give the 77 K and 300 K values of R_H, carrier concentration (n or p), mobility and resistivity for a series of PbTe epilayers grown, both with or without a substrate bias, at substrate temperatures of 180 ^{0}C, 260 ^{0}C, 330 ^{0}C and 410 ^{0}C. It is clear from the sign of the Hall coefficient that samples prepared at 330 ^{0}C and 410 ^{0}C, irrespective of the substrate bias are n-type whereas samples prepared at 180 ^{0}C and 260 ^{0}C are p-type, thus validating the hypothesis of ref (29).

While it is clear from tables 4.2-4.4 that the growth temperature provides a means of controlling the conductivity type of PbTe epilayers, no systematic dependence of the carrier concentration of either the n-type or the p-type samples on any deposition condition could be observed. Most of the samples exhibited high carrier concentration and were found to be degenerate as evidenced by the temperature-insensitive Hall coefficient (fig. 4.6) and carrier concentration (fig. 4.5). A few samples such as 32(b) exhibited low carrier concentration at 77 K ($\approx 2\times 10^{17} cm^{-3}$) and a temperature dependent Hall coefficient; however, the growth conditions leading to such samples were not precisely identified and further studies are needed to optimize the growth conditions to obtain PbTe epilayers with controllable and more intrinsic-like carrier concentrations. We note that other workers have also observed degenerate (temperature independent) behavior in PbTe samples with high doping levels [12,17,44].

A comparison of Tables 4.2, 4.3 and 4.4 with Table 4.1 shows that the 77 K mobility values for sputter-deposited samples 36(d), 33(e) and 40(a) are quite comparable to samples of similar carrier concentration prepared by other epitaxial growth techniques. Allgaiers and Houston[36] have observed for PbTe films, that at a given temperature, the lattice mobility was independent of the carrier concentration at low carrier concentrations, gradually decreased at higher concentrations, and varied inversely with carrier concentration for carrier concentration $\simeq 5\times 10^{19} cm^{-3}$.

However, as can be seen from Tables 4.2-4.4, there is a wide variation n in the mobility values for samples with similar carrier concentration. The mobilities in PbTe films may be expected to be limited by the thickness of the film due to surface scattering. However, we did not observe any systematic variation with thickness in the sputter-deposited samples prepared for this study. We should emphasize though that layer thickness was not a controlled parameter and also that the samples for this study were grown primarily for investigating the dependence of conductivity type on deposition conditions and no effort was made to optimize the growth conditions to achieve high mobilities. Nonetheless, to determine the scattering mechanism responsible for limiting the mobilities in these films, the Hall mobility for a few selected samples of different carrier concentration (fig. 4.7) was analyzed using Equation ($1/\mu_{exp} = 1/\mu_L + 1/\mu_I + 1/\mu_n$). The temperature dependence of the mobility for samples 36(d), 38(a) and 40(c) could be fitted assuming a combination of acoustic phonon scattering, ionized impurity scattering and neutral impurity scattering. The low-temperature mobility for these samples was found to be limited by the temperature independent neutral impurity scattering. Vaya et al.[12] have also observed similar behaviour for HWE PbTe films. These neutral impurity scattering centers could be crystal defects, the free Pb or Te atoms or other unknown impurities. The fit to the mobility data for sample 32(b) was not very good, particularly at the higher temperatures and this may be due to a temperature dependent effective mass or grain boundary scattering or both and needs further study.

Technique used	Mobility $cm^2V^{-1}s^{-1}$	Carrier Concentration cm^{-3}	Hall Coeff cm^3/c	Reference
HWE	$4.2 \times 10^4_{(77K)}$	$\approx 10^{18}$	9.0	13
MBE				
$Asgrown_{p-type}$	1.65×10^4	6.8×10^{16}	-	36
$Annealed_{n-type}$	2.8×10^4	3.4×10^{17}		
Vacuum	$\approx 6 \times 10^2_{(300K)}$	1.2483×10^{19}	5.0	20
Evaporation	$\approx 9 \times 10^2_{(77K)}$			
HWE				15
undoped	$3.5 \times 10^4_{(77K)}$	5.0×10^{17}	-	
Te-doped(p-type)	$1.6 \times 10^4_{(77K)}$	5.5×10^{17}		
Bi-doped(n-type)	$1.05 \times 10^4_{(77K)}$	8.1×10^{18}		
TI-doped(p-type)	$8.5 \times 10^4_{(77K)}$	5.0×10^{18}		

Table 4.1: Electrical properties of PbTe epilayers grown by various techniques

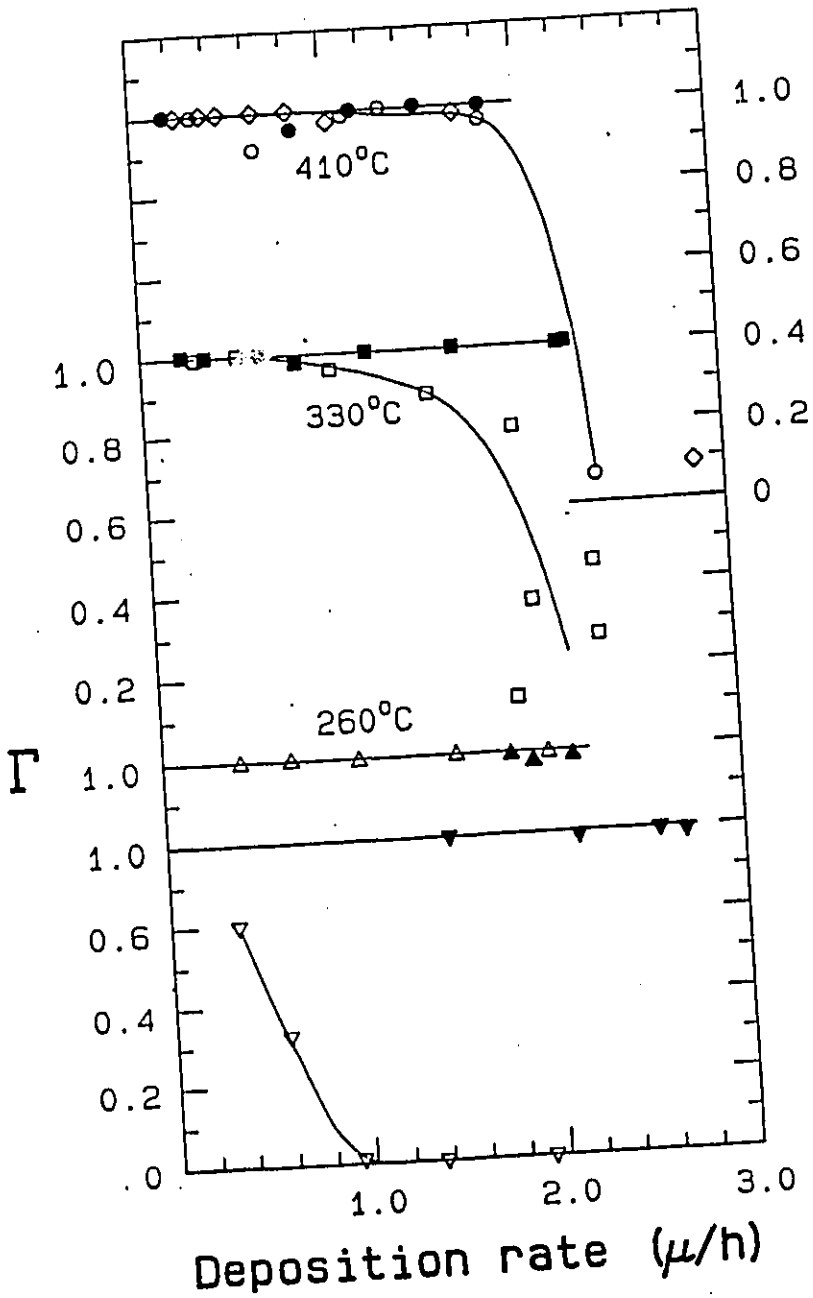

Figure 4.1: Γ versus rate of deposition at different T_s

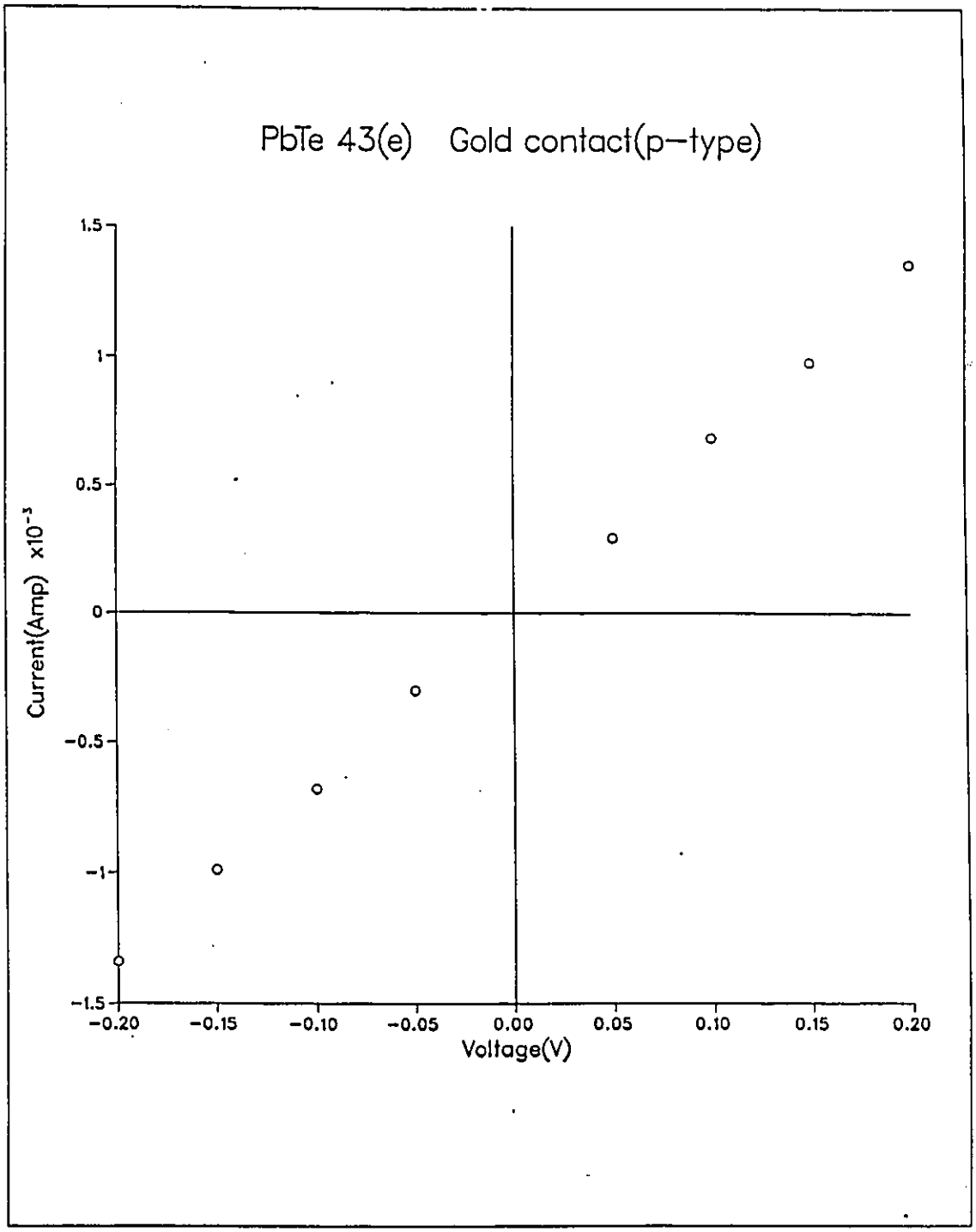

Figure 4.2: I-V characteristics of sputtered p-type PbTe films

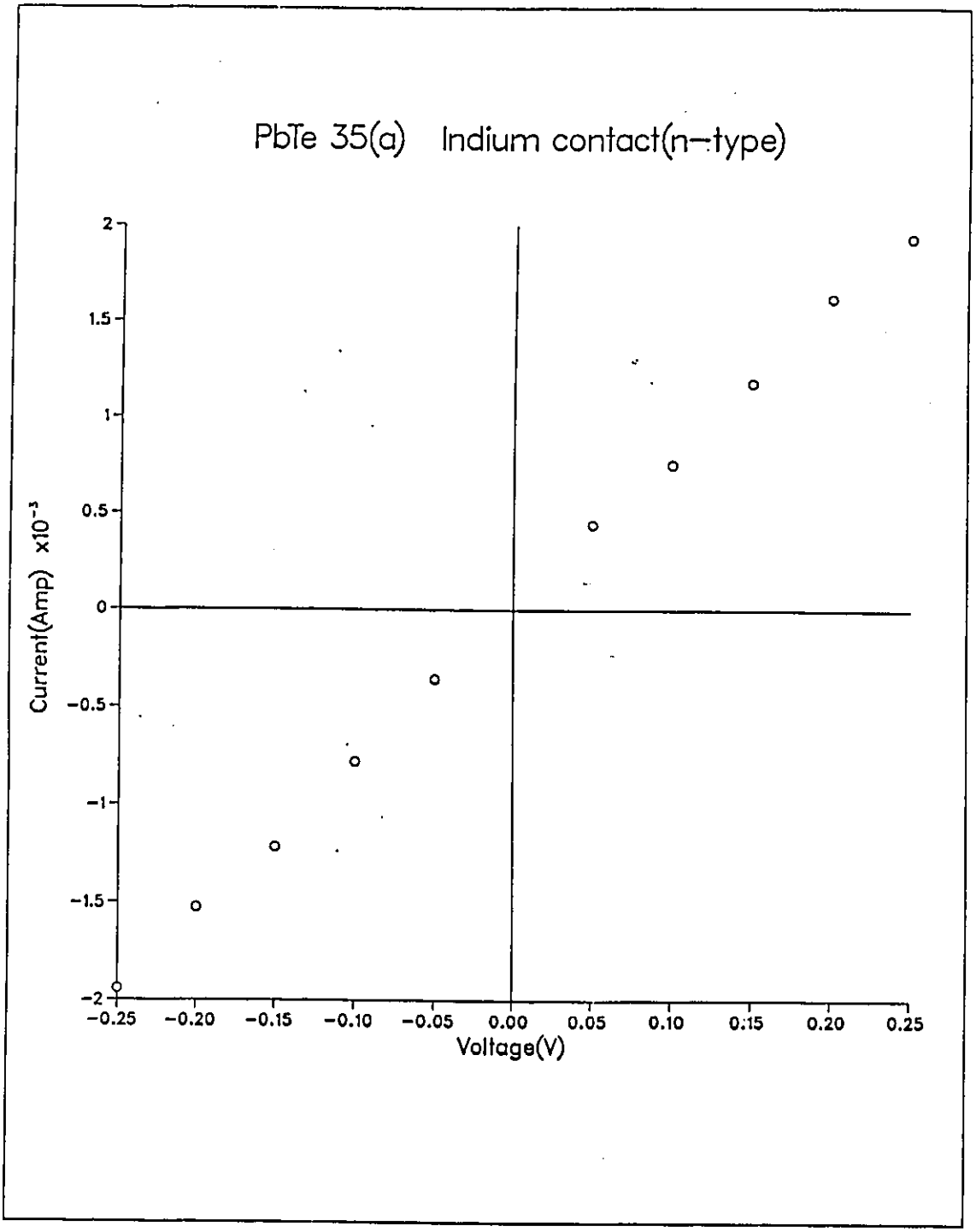

Figure 4.3: I-V characteristics of sputtered n-type PbTe films

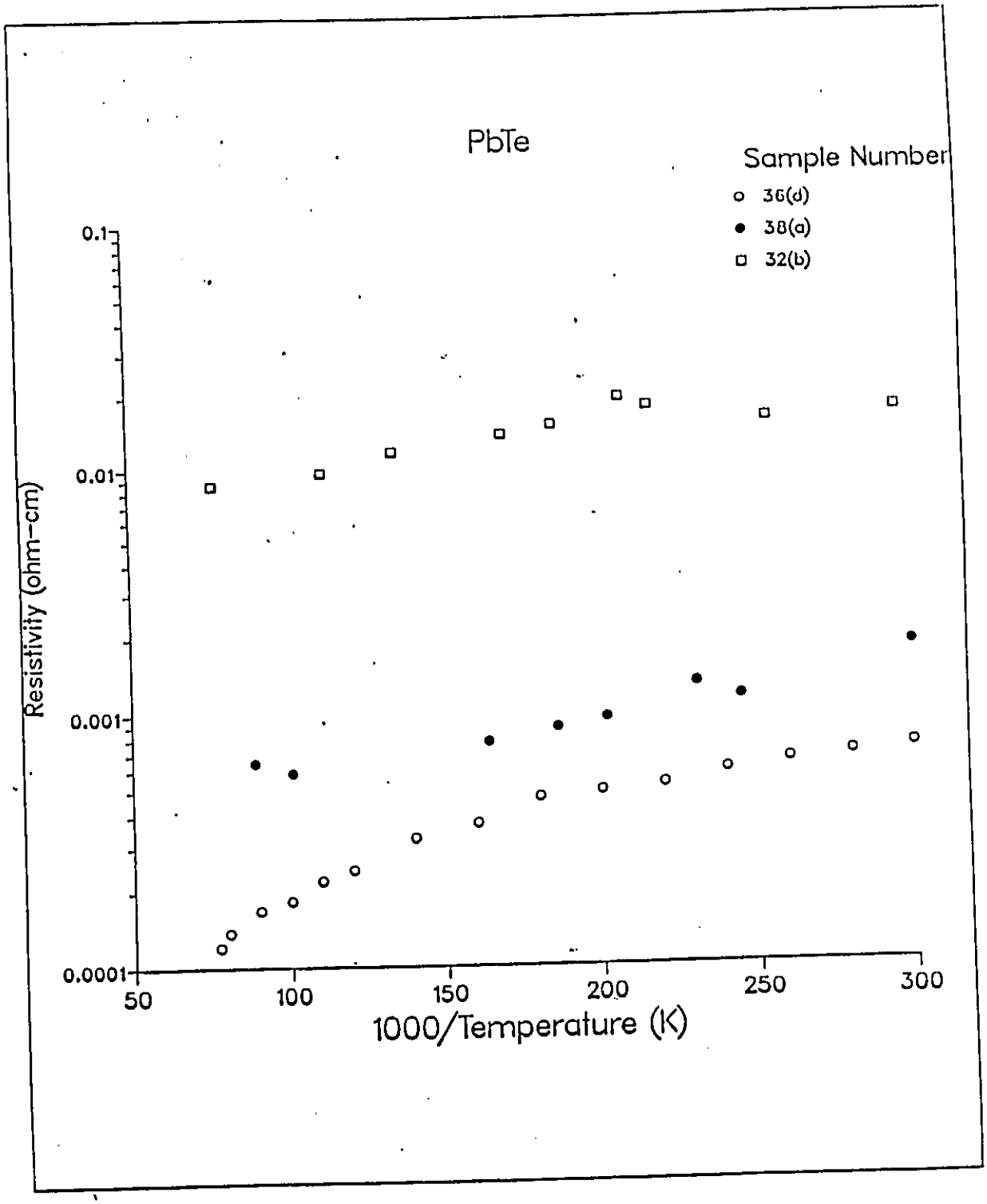

Figure 4.4: Resistivity vs 1000/T for sputtered n-type PbTe films

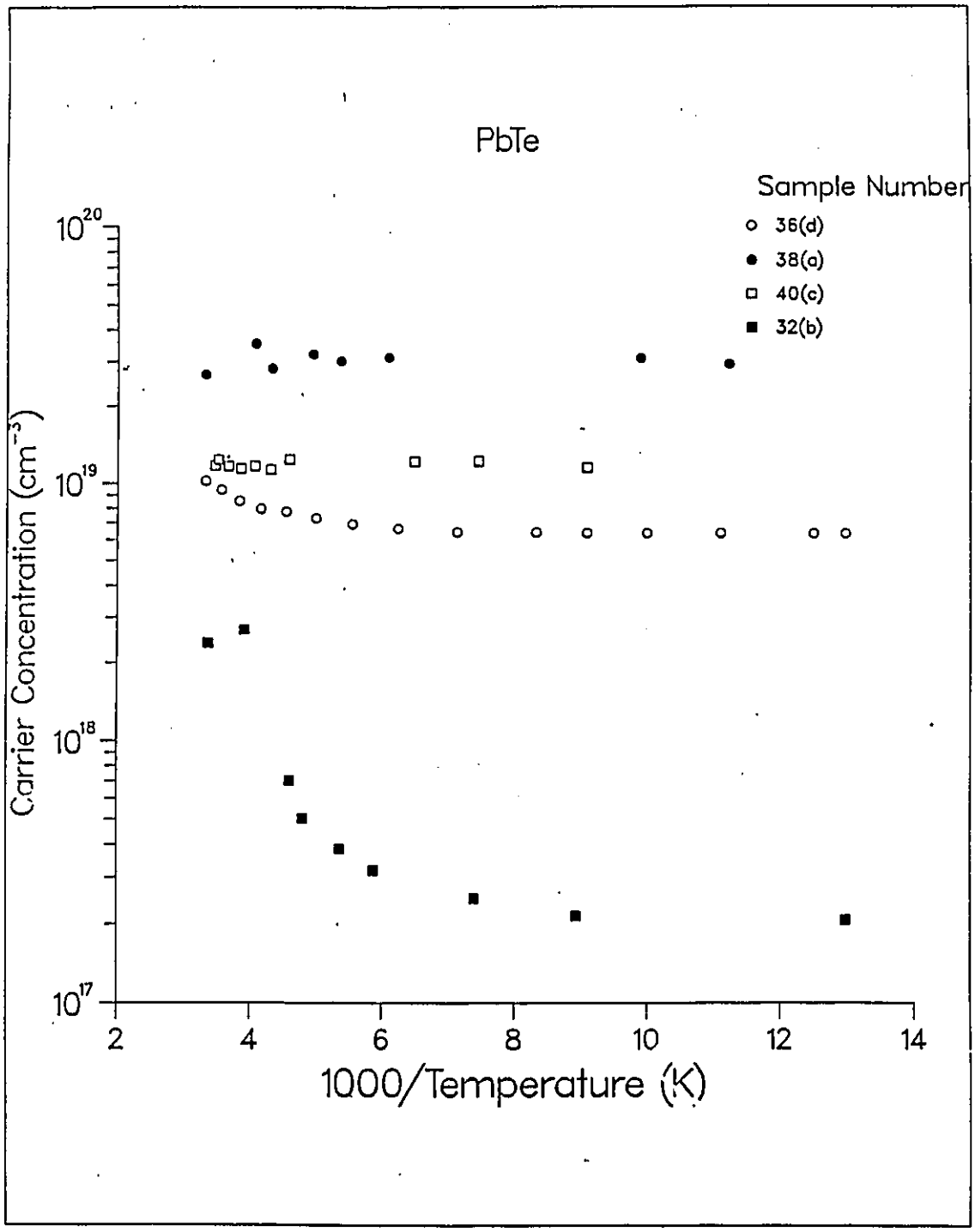

Figure 4.5: Carrier concentration versus 1000/T for sputtered n-type PbTe films

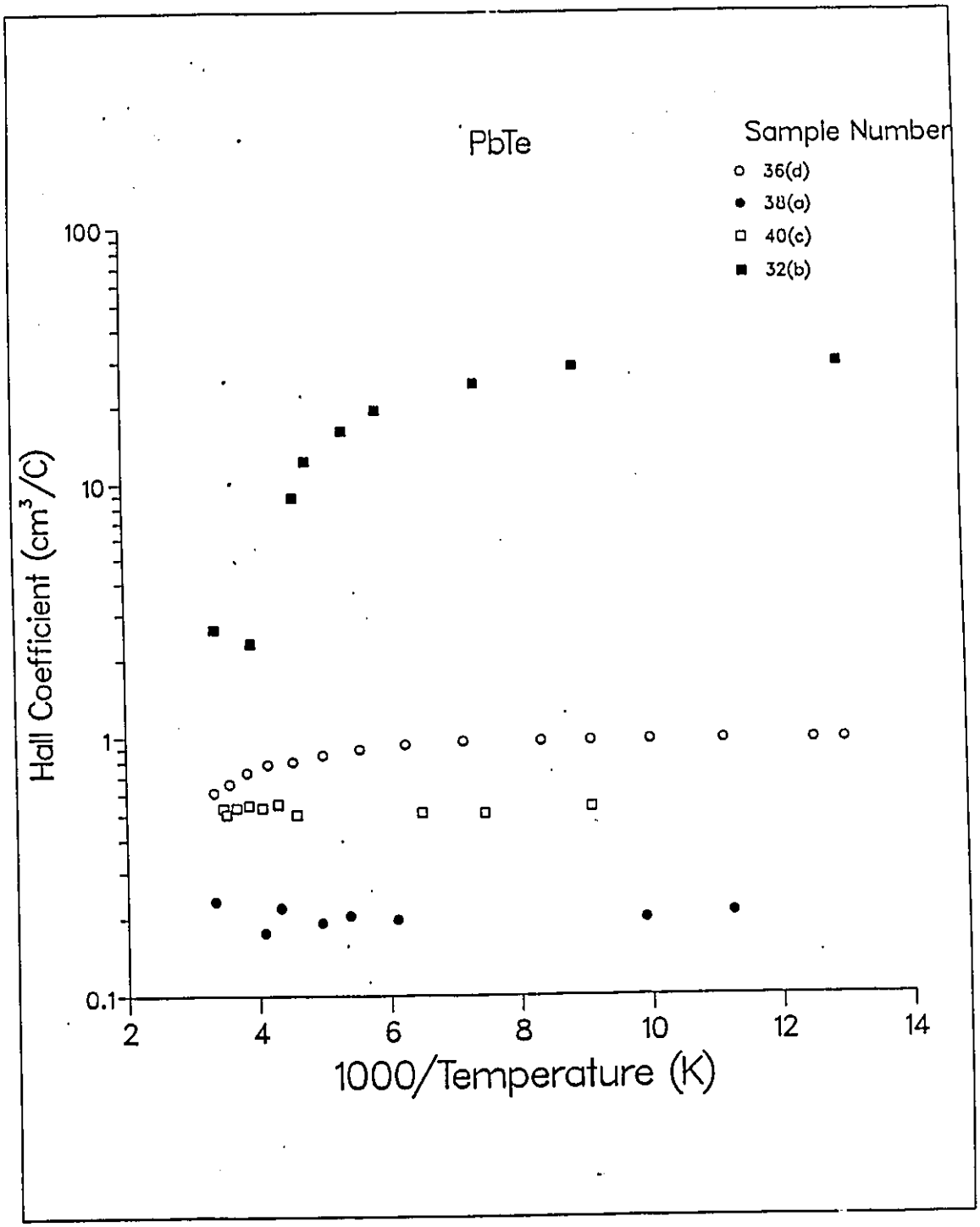

Figure 4.6: Hall coefficient versus 1000/T for sputtered n-type PbTe films

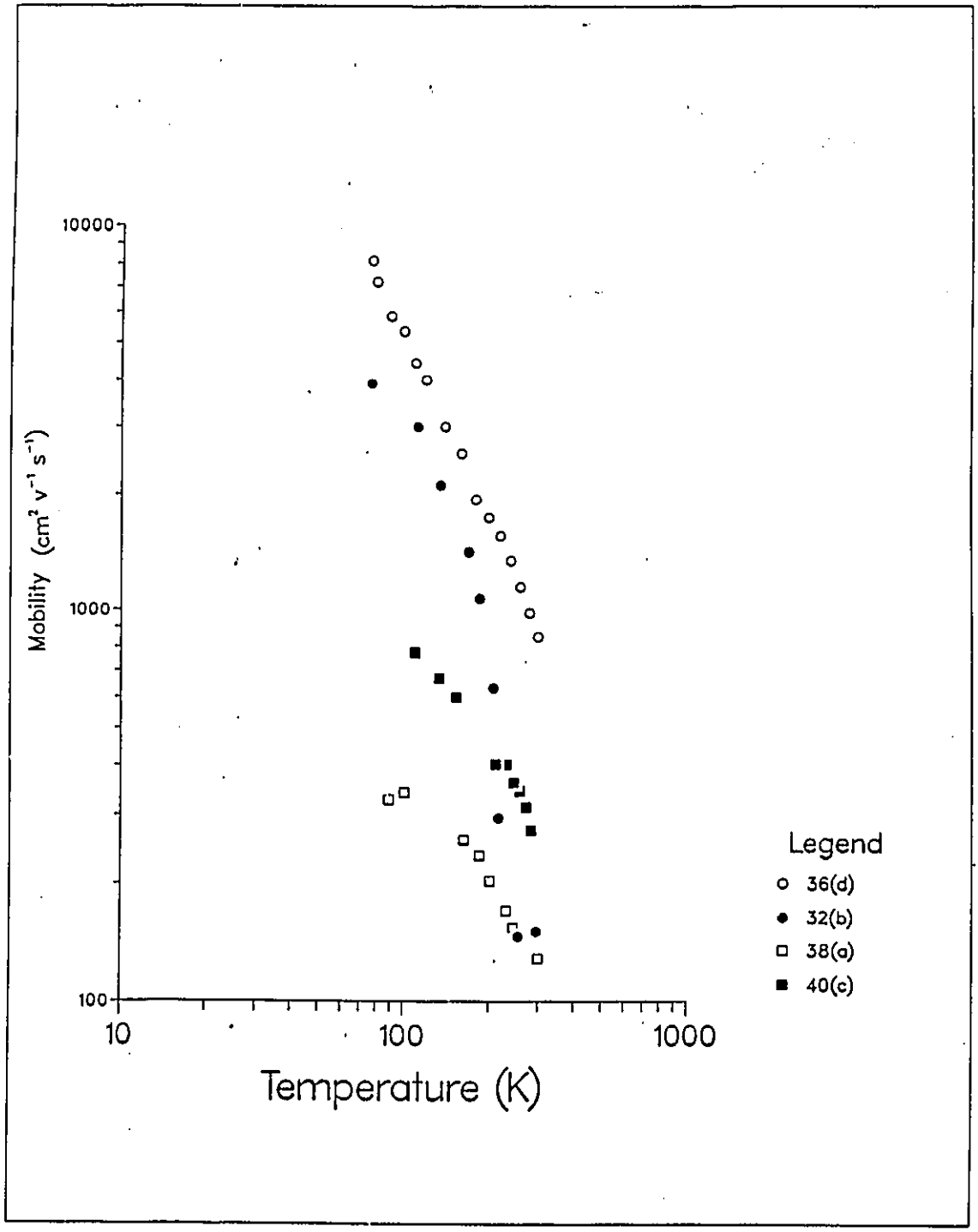

Figure 4.7: Mobility vs T for sputtered n-type PbTe films

Sample /Temp.	T_s (C)	V_{sub} (V)	t μm	R_H cm^3/C	n,p cm^{-3}	μ $cm^2V^{-1}s^{-1}$	ρ $\Omega - cm$
33(e)	410	0	1.02				
77K				-.99	6.3×10^{18}	7685.3	1.3×10^{-4}
300K				-.98	6.3×10^{18}	727.2	1.3×10^{-3}
33(c)	410	0	3.37				
77K				-.48	1.3×10^{19}	1051.5	4.8×10^{-4}
300K				-.45	1.4×10^{19}	267.3	1.7×10^{-3}
35(a)	410	-10	3.45				
77K				-1.50	4.1×10^{18}	2136.7	7.0×10^{-4}
300K				-1.13	5.5×10^{18}	317.5	3.5×10^{-3}
40(a)	410	-10	.92				
77K				-.79	7.9×10^{18}	4071.3	1.9×10^{-4}
300K				-.51	1.2×10^{19}	405.3	1.2×10^{-3}
42(b)	330	0	6.91				
77K				-.40	1.5×10^{19}	417.1	9.6×10^{-4}
300K				-.22	2.8×10^{19}	150.1	1.4×10^{-3}
42(c)	330	0	5.74				
77K				-.29	2.1×10^{19}	721.8	4.1×10^{-4}
300K				-.14	4.3×10^{19}	189.1	7.7×10^{-4}

Table 4.2: Electrical properties of r.f. magnetron sputtered PbTe samples

Sample /Temp.	T_s (C)	V_{sub} (V)	t μm	R_H cm^3/C	n,p cm^{-3}	μ $cm^2V^{-1}s^{-1}$	ρ $\Omega - cm$
37(e)	330	0	.875				
77K				-.86	7.2×10^{18}	517.1	1.6×10^{-3}
300K				-.74	8.5×10^{18}	203.6	3.6×10^{-3}
37(d)	330	0	1.82				
77K				-1.25	4.9×10^{18}	421.3	2.9×10^{-3}
300K				-1.10	5.6×10^{18}	113.6	9.7×10^{-3}
37(c)	330	0	2.95				
77K				-.99	6.3×10^{18}	799.8	1.2×10^{-3}
300K				-.86	7.2×10^{18}	345.7	2.5×10^{-3}
38(a)	330	-10	1.08				
77K				-.21	2.9×10^{19}	327.6	6.4×10^{-4}
300K				-.23	2.6×10^{19}	128.3	1.8×10^{-3}
36(d)	330	-10	1.02				
77K				-.98	6.3×10^{18}	8147.3	1.2×10^{-4}
300K				-.61	1.0×10^{19}	851.2	7.2×10^{-4}

Table 4.3: Electrical properties of r.f. magnetron sputtered PbTe samples

Sample /Temp.	T_s (C)	V_{sub} (V)	t μm	R_H cm^3/C	n,p cm^{-3}	μ $cm^2V^{-1}s^{-1}$	ρ $\Omega - cm$
38(b)	330	-10	.81				
77K				-.69	9.0×10^{18}	1978.2	3.5×10^{-4}
300K				-.50	1.2×10^{19}	215.4	2.3×10^{-3}
41(a)	260	0	6.01				
77K				.71	8.8×10^{18}	625.1	1.1×10^{-3}
300K				.60	1.0×10^{19}	305.7	1.9×10^{-3}
39(c)							
300K	260	-10	1.81	.3834	1.6×10^{19}	183.6624	2.3878×10^{-3}
43(e)	180	0	1.05				
77K				.77	8.1×10^{18}	465.4	1.6×10^{18}
300K				.65	9.6×10^{18}	251.2	2.6×10^{-3}
44(b)	180	-10	1.29				
77K				.94	6.6×10^{18}	1047.6	9.0×10^{-4}
300K				.85	7.3×10^{18}	462.4	1.8×10^{-3}

Table 4.4: Electrical properties of r.f. magnetron sputtered PbTe samples

4.3 Conclusion

Hall measurements on sputter-deposited epitaxial PbTe films have confirmed that samples prepared at high growth temperatures (330 ^{0}C and 410 ^{0}C) are n-type and those grown at low substrate temperatures (180 ^{0}C and 260 ^{0}C) are p-type, irrespective of the substrate bias during growth. However, the carrier concentration values are generally high and do not exhibit a systematic variation with deposition conditions.

The Hall mobilities in some of the sputter-deposited films are comparable to values obtained on films with similar carrier concentrations grown by other techniques. The low temperature mobility values in the sputter-deposited samples are found to be limited by a temperature-independent neutral impurity scattering mechanism. The neutral impurities have not been identified but could be structural defects. One of the features of heteroepitaxial growth is the existence of a large density of structural defects at the interface due to lattice mismatch. The density of these defects is observed to decrease with film thickness along the growth direction and thus films with higher thickness exhibit high bulk-like mobilities.

The lack of control on the carrier concentration as well as the mobilities indicate the need to optimize the deposition conditions and grow thicker films. Such an effort is currently underway.

Bibliography

[1] Zanio, K., Semiconductor and Semimetals, vol.13, Academic press, New York (1978).

[2] Holloway, H., Physics of Thin Films, vol. 11, Academic press, New York (1980).

[3] Bicknell, R.N., Giles-Taylor, N.C., Yanka, R.W., Schetzina, J.F., Magee, T.J., Leung, C., Kawayoski, H. and Woolhouse, G.R., J.Vac.Sci.and Technol.,B 2 (1984) 417.

[4] Matsumura, N., Ohshima, T., Saraie, J. and Yodogawa, Y., J. Crys. Growth 71(1985)361.

[5] Ballingal, J.M., Wroge, M.L. and Leopold, D.J., Appl. Phys. Lett., 48 (1986) 1273.

[6] Schikora, D., Sitter, H., Humenberger, J. and Lischka, K., Appl. Phys. Lett. 48 (1986) 1276.

[7] Magee, R., Cheung, J.T., J. Vac. Sci. and Technol. A 1 (1983) 1604.

[8] Pessa, M., Jytha, O., Huttunen, P. and Herman, M.A., J. Vac. Sci. Technol. A 2 (1984) 418.

[9] Takaoka, H., Matsubara, K. and Takagi, T., Proc. Int'l Ion Engg. Congress, ISIAT'83 and 'IPAT'83, Kyoto (1983) p. 1241.

[10] Yoshij, K., Yoshinori, E. and Toshiya, H., Thin Solid Films, 147 (1987) 75.

[11] Hwang, S., Harper, R.L., Harris, K.A., Giles, N.C., Bicknell, R.N., Cook, J.W., Jr., Schetzina, J.F. and Chu, M., J. Vac. Sci. Technol. A 6 (1988) 2821.

[12] Vaya, P.R., Majhi, J., Gopalan, B.S.V. and Dattatreyan, C., Applications of Surface Science, 22/23 (1985) 731.

[13] Vaya, P.R., Majhi, J., Gopalan, B.S.V. and Dattatreyan, C., Phys. Stat. Solidi (A) 87 (1985) 341.

[14] Clemens, H., J. Cryst. Growth, 88 (1988) 236.

[15] Clemens, H., Fantner, E.J., Ruhs, W. and Baur, G., J. Cryst. Growth, 66 (1984) 251.

[16] Zimmermann, P.H., Mathews, M.E. and Joslin, D.E., J. Appl. Phys. 50 (1979) 5815.

[17] Zemel, J.N., Jensen, J.D. and Scholar R.B., Physical Review, 140 (1965) A 330.

[18] Semilotov, S.A., Suleimanov and N.A., Nuriev, I.R., Sov. Phys. r, Crystallogr, 25 (1980) 502.

[19] Mojejko, K. and Subotowiez, M., Thin Solid Films 8(1981) 319.

[20] Dawar, A.L., Janeja, O.P., Paradker, S.K., Kumar, P., Sachar, B.K. and Mathur P.C., J. Phys. Chem. Solids, 43 (1982) 267.

[21] Samiletov, S.A., Rakova, E.V., Zheludeva, S.I., Thin Solid Films, 66 (1980) 11.

[22] Manasevit, H.M., Ruth, R.P. and Simpson, W.I., J. Cryst. Growth, 77 (1986) 37.

[23] Willams, D., Parker, E.H.C., J. of Physics E, Scientific Instruments, 10 (1977) 1170.

[24] Kamlin A.N., Lakeenkov, V.M., Pelevin, O.V. and Shigaeva, S.M., Sov. Phys. Crystallogr., 27 (1982) 695.

[25] Lopez-Otero, A., J. Appl. Phys., 48 (1977) 446.

[26] Clemens, H., Ofner, P., Bauer, G., Hong, J.M. and Chang L.L., Materials Letters, 7 (1988) 127.

[27] Yoshino, J., Munekata, H. and Chang, L.L., J. Vac. Sci. Technol. B 5 (1987) 682.

[28] Das, S.R., Cook, J.G., Thin Solid Films, 163 (1988) 409.

[29] Das, S.R., Phipps, M., Boland, W.E. and Cook, J.G., Thin Solid Films (in press)

[30] Aouadi, S., Master's Thesis, Dept. of Physics, University of Ottawa, 1989.

[31] Chopra, K.L., Das, S.R., Thin Film Solar Cells, Plenum Press, New York (1983).

[32] Bube, R., Photoconductivity of Solids, New York, London, John Wiley and Sons, Inc., 1960.

[33] Rose, L., Concept in Photoconductivity and Allied Problems, No. 19, Interscience Publishers, New York, London, 1963.

[34] Das, S.R., Rajan, K., Van Der Meer, P. and Cook, J.G., Can. J. Phys., 65 (1987) 864.

[35] Putley, E.H., The Hall Effect and Semiconductor Physics, Dover Publication, New York, 1968.

[36] Allgaier, R.S. and Houston, B.B., Jr., Proc. Int. Conf. Semicond., (1962), p.172.

[37] Madelung, O., Schulz, M., Landolt-Bornstein Series, Vol.22., Springer-Verlag (1983).

[38] Madelung, O., Schulz,M., Weiss, H., Landolt-Bornstein Series, Vol.17, Springer-Verlag (1983).

[39] Tosinori, T., Hiroshi T., Youichi K. and Kakuei M., Thin Solid Films, 126 (1985) 149.

[40] Chu, T.L., Chu, S.S., Firszt, F., Naseem, H.A. and Stawski, R., J. Appl. Phys. 58 (1985) 1349.

[41] Wang, C.H., Cheng, K.Y., and Yang,S.J., Appl. Phys. Lett. 46 (1985) 962.

[42] Bicknell, R.N., Myers, T.H., Schetzina, J.F., J. Vac. Sci. Technol. A 2 (1984) 423.

[43] Dawar, A.L., Jain, S., Mohammad, A.O., Krishna, K.V., Mathur, P.C., Solid State Electronics, 22 (1979) 117.

[44] Holloway, H. and Logothetis, E.M., J. Appl. Phys., 42 (1971) 4522. Oct. 1971.

[45] Taylor, G.W. and Simmons, J.G., J. Phys.C: Solid State Phys., 7 (1974) 3067.

[46] Simmons, J.G. and Taylor G.W., J. Phys. C: Solid State Phys., 7 (1974) 3051.

[47] Spear, W.E., Loveland, R.J. and Al-Sharbaty, A., Journal of Non- Crystalline Solids, 15 (1974) 410.

[48] Chik, K.P., Lim, P.K., Tong, B.Y., John, P.K. and Gogna, P.K., Physical Review B, 27 (1983) 3562.

[49] Sun, Y.Z., Das, S.R., Williams, D.F. and Webb, J.B., J. Appl. Phys., 59 (1986) 3160.

[50] Nag, B.R., Electron Transport In Compound Semiconductors, Solid State Sciences, vol.11, 1980, Springer-Verlin, Berlin, Heidelberg, New York.